Potential for fresh submarine groundwater occurrence in an arid Mediterranean region: the case of Gulf of Gabes, Tunisia

Sarra Bachtouli[1,2], Mouna Abidi[1], Jean-Christophe Comte[3], Moncef Zairi[1*]

1: Ecole Nationale d'Ingénieurs de Sfax, University of Sfax, Tunisia

2: Faculté des sciences de Tunis, University of Tunis El Manar, Tunisia

3: School of Geosciences, University of Aberdeen, Scotland, UK

*: Corresponding author: moncef.zairi@enis.tn;

Abstract

Arid and semi-arid zones, including the southern Mediterranean countries, are among the world's most affected by water scarcity. Unconventional water resources, such as submarine fresh groundwater, may be key contributors to mitigate ongoing and future water crises for coastal regions and islands. In the Gulf of Gabes, Tunisia, several deep confined aquifers have been identified and the parts that are onshore have been well characterized. However, the offshore extension of these aquifers has been unexplored to date, except beneath Kerkenah and Djerba islands, where a number of exploitation wells are operating. In this work, the existing, but fragmented, geological, geophysical and hydrogeological data from both the marine and terrestrial sides of the Gulf of Gabes are synthesized for the first time in order to map the offshore extension of the deep aquifers and identify the quality of their groundwaters. Geological data confirmed the offshore continuity of the deep aquifers contained in the Miocene siliciclastic formations, particularly the Serravallian-Tortonian (ST) water-bearing horizon, on which the present research focuses more specifically, because of its wide extension and potential. In the study region, the ST aquifer is present onshore and is currently exploited in Kerkenah and Djerba islands. Offshore, the average thickness of the ST aquifer is about 200 m. Wireline log data suggest total porosity and salinity ranges of 30-36 % and 5.5-7.5 g/L, respectively. These conditions make the offshore water-bearing horizon of potential interest for agriculture, industry and domestic purposes, including after adequate treatments, such as desalination or dilution with freshwater.

Keywords: Submarine groundwater, offshore aquifer, geophysical methods, water supply, Tunisia

1 Introduction

The Mediterranean region is facing major difficulties related to limited groundwater resources, their widespread overexploitation and depletion, and the deterioration of their quality (Custodio and Bruggeman, 1987; Edmunds et al. 2003).. Meeting the growing water needs has become a challenge (Ritchie and Roser, 2017; Boretti, and Rosa, 2019). Semi-arid and arid regions such as the Southern Mediterranean countries are among the most affected by water scarcity (Tramblay et al., 2016) and at high risk in terms of future water security. Surface waters are scarce in these regions, and increasingly unreliable as a consequence of climate change causing more frequent and intense drought periods. Hence, secure water supplies are primarily relying on groundwater of highly variable geochemistry (Robertson, 1989; Dona et al., 2006; Cobbing et al., 2019), often dictated by local aquifer geological characteristics (Domenico and Schwartz, 1990; Guler and Thyne, 2004; Ayenew et al., 2008).

Tunisia has been suffering for several years of recurrent water shortages, which are worsening over time due to population growth and climate change. Tunisia is also characterized by irregular distribution of precipitation and surface water in time and space (Henia, 1993; Kingumbi et al., 2001). Overall precipitation is relatively low, varying from 1,500 mm yr^{-1} in the North to less than 100 mm yr^{-1} in the South. In response to fresh water scarcity, Tunisia has developed several management strategies (Ben Jemaa et al., 1998; Bouri and Ben Dhia, 2010; Kammoun et al., 2020) to ensure sustainable safe use of the resources for drinking, agricultural and industrial purposes including seawater desalination plants.

The utilization of unconventional water resources has become of increasing interest as one of the solutions to the ongoing and future water crises. Among them, submarine fresh groundwater and submarine groundwater discharge (SGD) are promising solutions particularly for coastal regions and islands (Bakker, 2006; Micallef et al., 2021). Submarine fresh groundwater refers to underground water found in aquifers beneath the seabed or coastal areas, and it has a low salinity level. Submarine groundwater discharge (SGD) is the means by which groundwater flows from the land or coastal areas into the sea.

In the 1960s, during petroleum exploration in the Atlantic Ocean off North America, offshore freshwater reservoirs were first discovered beneath the Florida continental shelf (Kohout, 1964). Since then, several researchers have compiled and analyzed global datasets and published regional coastal aquifer reviews, to elucidate the governing factors of offshore fresh groundwater bodies (e.g. Brown et al., 2001; Hensen et al., 2004; Mora, 2005; Lin et al., 2010; Hong et al., 2019; Weymer et al., 2020, Micallef et al., 2021). Post et al. (2013) showed that the presence of offshore fresh groundwater systems in continental shelves is globally widespread. Offshore fresh-to-brackish

groundwater, which the authors termed ‘freshened groundwater’, i.e. a slightly to moderately saline water (less than 10 g/L), have been confirmed in many continental shelves around the world (e.g. the Northeast United States, Suriname, South Africa, Peru, Greenland, Australia, Tanzania, Malta and New Zealand).

The majority of offshore freshened groundwater bodies are hosted in siliciclastic sedimentary aquifer systems with total porosities typically ranging between 30 % and 60 %. They occur in continental margins, where the sea is generally less than 200 m deep (Post et al., 2013; Knight et al., 2018; Micallef et al., 2021). According to Gustafson et al. (2019), Thomas et al. (2019) and Micallef et al. (2018), the main mechanism responsible for the formation of offshore freshened groundwater is the existence of meteoric freshwater recharge regardless of its geologic age, either from paleo-meteoric water or as modern meteoric water originating from recent or contemporary rainfall.

During the Earth’s history, coastal plains and shorelines migrated in response to global sea level oscillations (Lambeck and Chappell, 2001). The most recent low sea-level was during the Last Glacial Period (late Pleistocene to Holocene), which began about 1.5 Myr and ended about 15,000 years before present (BP) (Miller et al., 2012). The position of the relative level of the Mediterranean Sea during the Last Glacial Maximum, from 26,500 to about 19,000 years BP was around 115 m lower than today (Clark, et al., 2009, Jouet et al., 2006). The Messinian salinity crisis (Miocene-Cenozoic era, 5.97 Myr to 5.33 Myr BP), during which most of the Mediterranean Sea evaporated and the water level dropped more than 1,000 m (Krijgsman et al., 1999), has been proposed as one of the time periods having favorable conditions for the formation of freshened groundwater in the vastly emerged continental shelf (Krijgsman et al., 1999; Manzi et al., 2013; Kastner et al., 1990).

As a result of sea retreat, the paleo-morphology of the emerged coastal plains was reconfigured similarly to the current ones. The exposed lowlands hosted rivers and lake systems, depositing fluvial sediments and allowing meteoric recharge and groundwater flow processes (Middelburg and de Lange, 1989; Southgate and Möller, 2000; Zamrsky et al., 2020). During the subsequent transgression, the sea-level rise caused an abrupt change in sedimentary facies, depositing marine low-permeability to impermeable sediments, and hence creating confining conditions for the underlying fresh groundwater aquifers (Jouet et al., 2006).

The global shoreline position corresponds neither to the downstream boundary of terrestrial groundwater systems nor to the sea water boundary (Post, 2005). Seawater can penetrate onshore freshwater aquifers through a process known as seawater intrusion (SWI) (Xiao et al., 2018; Bachtouli and Comte, 2019) and fresh terrestrial water may discharge offshore through a process known as submarine groundwater discharge (SGD) (Bratton, 2010; Moore, 2010).. Hydrological studies (eg. Kooi and Groen, 2001; Bakker, 2006) have shown that, under active connections between onshore aquifers and sub-seabed geological formations, SGD can extend offshore far beyond the present

shoreline through long distance offshore freshened groundwater flow (OFG-flow) between layers of impermeable materials (Kooi and Groen, 2001; Knight et al., 2018; Weymer et al., 2020). According to Knight et al. (2018), OFG-flow differs from SGD in that the latter is recognized as direct groundwater discharge into the sea water. However, OFG-flow reflects preferential pathways for offshore freshened groundwater bodies within continental shelves, from onshore recharge to SGD. It also includes freshwater reaching the freshwater/seawater interface in the subsea bed sediments. Hydraulic gradients and topographic relief-driven fluid flow are the most important driving forces enabling fresh groundwater circulation to depths and towards the outward regions of the continental shelf where it has been discovered (Mulligan and Charette, 2009).

There is currently a growing interest by both scientists and water managers to explore and assess offshore freshened groundwater reserves as an alternative source of water, mainly for water-scarce coastal regions and islands. The presence of freshened water in the continental shelves may provide a high economic benefit for countries that depend on desalination as their main source of freshwater. Water desalination costs could be significantly reduced by the use of water with lower total dissolved solids (TDS) than seawater (Bertoni et al., 2020). The cost of desalting seawater with a TDS of 38 g/L range from $ 0.65 to $ 2.00 per m^3 and from $ 0.24 to $ 0.55 per m^3 for brackish groundwater with a TDS $\leq$ 10 g/L (WRA, 2012; Borghini et al., 2014; Arroyo and Shirazi, 2012).

In recent years, growth in industrial and agricultural activities has caused an increase in water demand met by groundwater abstraction throughout the Tunisian regions, which generated serious alteration of groundwater systems particularly in the South of the country (OSS, 2003, OSS 2005; Kamel et al., 2006) where weakly renewable or non-renewable groundwater reserves are the main water resource (Mamou and Kassah, 2002). Within the study area, groundwater serves as the primary water source for both the chemical industry centers located in the cities of Sfax, Skhira, and Gabes, as well as the main irrigated areas surrounding these cities and populations throughout the study region (Fig. 1).

The present study has been motivated by the recent efforts in advancing the knowledge and understanding of offshore freshened groundwater resources in Mediterranean countries where offshore fresh groundwater aquifers have been previously identified. The objective of this study is to provide regional evidence of the existence of offshore freshened groundwater bodies beneath the Tunisian continental shelf. This is achieved through compilation, synthesis and integrated analysis of extensive, yet fragmented, historical geological, geophysical and hydrogeological data acquired in both the terrestrial and the marine sides of the Gulf of Gabes.

2 Study area

The Gulf of Gabes in South-Eastern Tunisia spans between the region of Sfax to the North and the island of Djerba to the South. It covers an area of 35,900 km², with a shallow (less than 200 m deep) gently dipping continental shelf (Ben Othman, 1973). The Gulf of Gabes, including the Kerkenah and Djerba islands, has a coastline length of 715 km in the Mediterranean Sea (Fig.1).

The region has an arid to semi-arid climate influenced by dry and hot air masses coming from the Sahara Desert to the South, while exposed to humid air masses from the Mediterranean Sea to the North and East. The summer season (June to September) is dry and hot, and the winter months, from January to March, are wet and cool. The average temperature is about 11 °C in the winter and 23 °C during summer. The precipitation is highly irregular, with an average annual precipitation of less than 250 mm and high evapotranspiration rates of over 1700 mm yr^{1}. The deep groundwater resources in the study area are found as three main aquifer systems occurring within the Gabes sedimentary basin formations that were deposited between the Cretaceous and Holocene periods. These three deep aquifer systems are referred to as the Sfax deep aquifer, Gabes aquifer system, and Medenine aquifer system.

2.1 Structural and Geological context

The Gulf of Gabes basin has recorded different paleo-tectonic events that have affected the region since the Paleozoic Era.

The Sfax region is characterized by a series of long-wavelength NE-SW anticlines, controlled by faults. In contrast, the Gabes region is characterized by a chessboard-like topography with horst and graben structures bounded by the directions of the main faults (Fig.1). The Jeffara of Gabes basin is a collapsed block inclined towards the Mediterranean coast, with elevations not exceeding 150 m. The Jorf-Zarzis-Djerba region is situated at the southern extremity of the Gulf of Gabes. It is a part of Jeffara of Medenine basin with a structural style of a collapsed block separated from the Dahar Plateau by the Medenine fault (Benton et al. 2000; Bouaziz et al. 2002).

The Jorf, Zarzis and Djerba Island region is a flat area affected by numerous faults orientated NW-SE, inherited from extensional tectonic events, with a maximum elevation of 54 m in the South of the Djerba Island. The offshore side of the Gulf of Gabes basin has a horst and graben structure bordered by lystric NW-SE normal faults (Bédir, 1995). The NW-SE faults seem to be developed as part of the extensional tectonic during early Permian (Pe) to Triassic (T) rifting phases (Fig.1). These structural features predominantly influenced the depth and geometry of aquifer reservoirs and their hydraulic connections, particularly in the Gabes and Medenine regions.

The different stratigraphic horizons, reflecting the sedimentary succession that deposited since the Upper Permian throughout the Gulf of Gabes, have been identified from seismic profiles and from borehole lithological data. Onshore, outcrop geology maps of the Gulf of Gabes show that the Mio-Plio-Quaternary (MPQ) siliciclastic materials are the dominant lithology (Castany, 1951, 1954; Burollet, 1956; Busson, 1967; Bouaziz, 1995,). Figure 2 shows a simplified lithostratigraphic log for the region of the Gulf of Gabes. The middle Miocene (MM) horizons are made of alternating clay, sand and sandstone with a fluvio-deltaic environment. The upper Miocene (UM) horizon includes the continental facies of sandy formation and the marine facies of peri-reef environment composed of fossiliferous limestone strata (Biely et al., 1972, Ben Ferjani et al., 1990).; Moktar and Mannaï-Tayech, 2014).

2.2 Hydrogeological setting

The main aquifers of the region are: 1/ The Sfax deep aquifer (SDA), mainly composed of Miocene sand and sandstone (Serravallian-Tortonian). 2/ The Gabes aquifer system, composed of Turonian (Tu) and Senonian (Se) carbonate layers (limestone and dolomite) and a Serravallian-Tortonian siliciclastic layer (STG). 3/ The Medenine aquifer system, composed of a Triassic (T) siliciclastic aquifer, Jurassic (J) carbonate aquifer and Serravallian-Tortonian siliciclastic aquifer (STZ).

The Gabes and Medenine deep aquifers are hydraulically interconnected with groundwater flow from one aquifer to another (Fig. 2).

2.2.1. Sfax deep aquifer (SDA)

The SDA extends across the Sfax region from onshore to the Kerkenah Islands, covering an area of approximately 7,500 km² with about 235 km of Mediterranean coastline (Fig.3). The Serravallian-Tortonian (ST) formations make up the main deep aquifer reservoir, composed of sand and sandstone interbedded with clay. The Northern boundary of the continental (onshore) part of the SDA corresponds to the major impervious East-West fault of Ksour Essaf. Its Western boundary coincides with the North-South axis. In its Southern part, the aquifer system partially connects to the Gabes aquifer system in the Skhira region. A superficial phreatic aquifer exists in the Mio-Plio-Quaternary undifferentiated siliciclastic layers above the SDA. Its groundwater is mostly saline offshore but freshwater occurs onshore forming a coastal wedge and as a lens beneath Kerkenah islands. The aquifer has a lenticular aspect, with lateral and vertical variations over depth and water-bearing layers. The phreatic aquifer has limited freshwater resources due to the low meteoric recharge and a relatively high salinity of groundwater overall.

It is highly vulnerable to groundwater contamination from human activities and seawater intrusion in the coastal and offshore areas (Trabelsi at al., 2007). Figure 3 illustrates a conceptual model of the SDA (AB cross-section on Fig.1) and the superficial local aquifer. This scheme is also encountered, with some modifications, in the aquifer systems of the Gulf of Gabes.

Borehole lithological data show that the thickness and depth of the SDA water-bearing ST horizon vary across the Sfax region. Average thickness is 250 m buried at depths from 200 m to more than 350 m as indicated in the cross sections of Fig. 4. The maximum thickness has been recorded in the central part of the region, and gradually decreases towards the Northern and Southern borders (Fig. 4 a). In the NW-SE direction, the ST thickness is less variable as shown on the cross-section EF in Fig. 4-b.

The increasing water demand associated with economic and social growth in the Sfax region has made the SDA one of the main resources for water supplies in the region.

The exploitation of the SDA aquifer went from an average of 10 million (M)m^3 for the period 1980-1986, increasing significantly from 1987, to reaching over 35 Mm^3 in 2018 (Fig. 5).

Since 1987, the rapid increase of water consumption has resulted in intensive exploitation of the aquifer, leading to declines of groundwater levels, as shown in Fig. 6 for the period 2000-2018 (DGRE, 2018 b). The average rate of water-level decline in the SDA is about 0.6 m $year^{-1}$ over the considered observation period.

Currently, the annual abstraction volume for agriculture, industry and domestic usages is about 85 % of the SDA's estimated annual renewable resources. The average abstraction is close to 30 Mm^3 $year^{-1}$ while the amount of lateral inflow is estimated to be 35 Mm^3 $year^{-1}$ (DGRE, 2018 a), coming mainly from neighboring aquifers. The SDA discharge to the Mediterranean Sea was estimated to be approximately 23 Mm^3 $year^{-1}$ (CRDA Sfax, 2005). The SDA is characterized by a salinity between 2.7 g/L and 10.3 g/L (Fig. 7), with highest values found in the Skhira region (CRDA Sfax, 2005; Trabelsi et al. 2007).

2.2.2 The Gabes aquifer system

The Gabes aquifer system covers an area of about 7,200 km^2. It consists of a multi-layered system with variations in lithological composition, thickness and depth of water-bearing horizons. It is mainly formed by the Senonian (Se) and Turonian (Tu) carbonate formations and the ST siliciclastic formation. The Se aquifer is the main

exploited aquifer in the region. It is divided into two lithostratigraphic horizons: the lower one, marked by karstic gypsum and layers of low-permeability marls of approximately 50 m thickness, followed by a limestone horizon of variable thickness, up to 500 m. The Tu aquifer horizon is composed of dolomites and fissured limestones, with constant thickness rarely exceeding 50 m. The ST aquifer of the North of Gabes (STG) is formed by the fluvial materials of Begluia Formation (Bouaziz, 1995; Benton et al., 2000). It is hosted by a fine- to coarse-grained sandstones horizon of variable thickness from 25 to 80 m, increasing toward the Mediterranean Sea direction.

The Jeffara of Gabes basin is affected by high fault density, as a result of extensive tectonic activities during the Mesozoic era (Bouaziz, 1995) creating a vertical compartmentalization of the Gabes aquifer system. The structural configuration influences the hydrodynamic behavior of the aquifer system and connections between the different water-bearing horizons (Fig. 8). According to the OSS (2005), these aquifers are recharged at 75 % by groundwater inflow from the neighboring Continental Intercalary (CI) mega-aquifer. The remainder comes from rainfall infiltration, through the outcropping Miocene formation. The mean annual inflow is estimated to be 74.7 $Mm^3\ y^{-1}$ (Abidi, 2004).

The CI is considered as a fossil aquifer with non-renewable groundwater resources hosted within the detrital sediments of the Asfer group deposited during the Lower Cretaceous epoch (Neocomian-Albian). This aquifer is formed by a succession of cross stratified sandstones intercalated with clay-rich strata. The CI has a maximum thickness of 1,500 m (Edmunds et al. 2003).

The previous multidisciplinary studies confirmed the existence of a lateral communication between the CI and the Gabes aquifers through the El Hamma active fault, oriented N-S and NW- SE (Abid et al., 2011; Abid et al., 2012). The hydraulic heads of the CI aquifer indicate W to E groundwater flow. The CI artesian pressure head near El Hamma fault is about 200 m compared with only 50 m in the neighboring aquifers (OSS, 2003), implying discharge of the groundwater from the former aquifer into the latter (Mekrazi, 1975; Mamou, 1990; Sahli et al., 2013). Driven by hydraulic potential gradients, groundwaters of the Tu and Se aquifers, in turn, discharge into the uppermost STG via NE-SW and E-W fault networks (Sahli et al., 2013).

Groundwater samples of the Gabes aquifer system exhibit a salinity between 0.8 g/L and 4.9 g/L, while the STG exhibits salinities between 2.9 g/L and 4.9 g/L (Fig. 9). The exploitation survey shows an abstracted annual volume of groundwater of about 92.4 % of the total annual renewable resource, i.e. the total annual abstraction was estimated to be 106.5 $Mm^3\ year^{-1}$ compared to a recharge rate by lateral inflow estimated to be 115.3 $Mm^3\ year^{-1}$ in 2018 (Fig .9). Of these 106.5 $Mm^3\ year^{-1}$, it is estimated that over 71% comes from the Se horizon (more than

75 Mm^3 $year^{-1}$). However, the average abstraction from the STG is close to 16.5 Mm^3 $year^{-1}$ (DGRE, 2018 a). The SGD is about 58 Mm^3 $year^{-1}$ (Abidi, 2004)

The temporal evolution of water-table depth between 2005 and 2018 in the STG (see Fig. 10) shows a continuous decline from about 37 m to 49 m and 34 m to 45 m in P17 and P20, respectively (DGRE, 2018 b) with an average drawdown of 0.85 m $year^{-1}$.

2.2.3. The Medenine Aquifer System

The Medenine aquifer system is composed of three aquifer horizons: The Triassic sandstone aquifer of the Sahel El Abebssa (T); the Jurassic carbonate aquifer of Zeuss□Koutine (J) composed of limestone and dolomite; and the ST aquifer of Jorf-Zarzis-Djerba region (STZ). These aquifers are hydraulically connected, making up the largest confined aquifer in the Jeffara of Medenine basin (OSS, 2006; Hamzaoui Azaza et al., 2013). The STZ covers the area between the two peninsulas of Jorf and Zarzis and extends to the Djerba island. The STZ covers approximately 2,800 km^2, including 514 km^2 in the Djerba Island with a total coastline of about 350 km. It is a confined water-bearing horizon, consisting of sandy material of the Begulia Formation. The aquifer thickness varies from 45 to 300 m. It is confined beneath the Mio-Plio-Quaternary sediments composed of marl, sand, clay and gypsum intercalations, reaching 250 m in thickness (Fig. 11).

The STZ receives annually an overall recharge of 22.1 Mm^3 (DGRE, 2018 a) with an estimated abstraction of 0.6 Mm^3 $year^{-1}$, 9.2 Mm^3 $year^{-1}$, and 12 Mm^3 $year^{-1}$, n Jorf peninsula, Zarzis peninsula and Djerba Island, respectively. The recharge takes place through lateral water leakage via faults. The STZ is recharged by inflow from the J aquifer, which in turn is recharged by groundwater from the T aquifer through the Tajra fault. Hence, groundwater flows from the Southwest (older aquifers) to the Northeast (younger aquifer), crossing Jorf and Zarzis peninsulas to Djerba Island.

Early measurements (2018) showed a large range of variation in groundwater salinity of the Medenine aquifer system, between 0.5 g/L and 7.8 g/L (Fig. 12). Groundwater salinity of the STZ aquifer varies from 5 g/L to 5.6 g/L in Jorf peninsula, from 5.6 g/L to 7.4 g/L in Zarzis peninsula, and from 4.9 g/L to 7.8 g/L in Djerba Island. The groundwater usage in Medenine region has grown tremendously during the past three decades. Currently, over 70 % of groundwater resources in Medenine region are exploited compared to 50 % during the period before the 1980s (Trabelsi, 2009, DGRE, 2018a). The SGD is about 40 Mm^3 $year^{-1}$ from the Medenine aquifer system to the Mediterranean Sea (OSS, 2005).

The total annual abstraction from the Medenine aquifer system is estimated to be 48.2 Mm^3 $year^{-1}$, compared to lateral inflow rate of 38.1 Mm^3 $year^{-1}$, and reflects therefore an overexploitation and mining of the groundwater resources, causing an increase in water depth from about 6 m to 14 m in P41 and from 6 m to 17 m in P45. Even though there is a gap in data between 2007 and 2018, due to interruption of groundwater monitoring in this period, the maximum drawdown rate is observed from 2007 to 2018 when the abstraction increased dramatically (Fig. 13). Groundwater abstraction rates in the STZ were estimated in 2018 to be 17.7 Mm^3 $year^{-1}$, including 0.7 Mm^3 $year^{-1}$, 8 Mm^3 $year^{-1}$ and 9 Mm^3 $year^{-1}$ in Jorf peninsula, Zarzis peninsula and Djerba Island, respectively (DGRE, 2018a).

3 Data and Methods

Several studies have been carried out to understand the hydrogeological behavior in the onshore part of the Gulf of Gabes aquifers (Abidi, 2004; Trabelsi et al. 2007; Sahli et al., 2013). However, the offshore extension has been unexplored to date. The present study constitutes a first attempt to provide clues of offshore freshened groundwater beneath the Tunisian continental shelf. Lithological, geophysical and hydrological data acquired in both onshore/offshore sides of the Gulf of Gabes are analyzed to set the map extent of the offshore part and to understand the connection between onshore and offshore water-bearing horizons.

3.1 Lithology data analysis

Lithostratigraphic data from 85 boreholes logs, including 14 petroleum boreholes logs from the offshore Gulf of Gabes, have been used to produce contour maps of the depth, the top and the base of the ST horizons, and an isopach map of their thickness. Data were collected from the DGRE (General Directorate of Water Resources, Tunisia) database and from the ETAP (Tunisian Company for Petroleum Activities) database. The 2D isopach maps were created through Kriging interpolation using Surfer Software (Golden Software, 2014).

3.2 Transmissivity and hydraulic conductivity data

Estimated transmissivity and hydraulic conductivity data were collected from literature for all aquifers of the SDA, Gabes aquifer system and the Medenine aquifer system. Transmissivity values were obtained from drawdown-pumping tests of available production wells. Hydraulic conductivity values were calculated directly as the ratio between transmissivity and aquifer thickness.

3.3 Piezometric data analysis

The groundwater monitoring network of the deep aquifer systems in the Gulf of Gabes is composed of 45 piezometers, with groundwater heads recorded since the 1980s. Analysis of historical piezometric data showed significant data gaps. These data were used for building piezometric maps through Kriging interpolation with Surfer, using the data of the most recent and complete piezometric survey carried out by the DGRE in 2018. Piezometric maps for the all hydrogeological systems in the Gulf of Gabes, including the SDA, the Gabes aquifer system and the Medenine aquifer system, were used to improve understanding of the processes responsible for land-sea water exchanges and the onshore-offshore groundwater flow relation.

3.4 Wireline log data analysis

Use of borehole wireline logging for aquifer characterization and groundwater behavior studies is relatively common practice (e.g. Muldoon et al., 2001; Williams et al., 2002). Electrical resistivity, spontaneous polarization (SP) and gamma-ray (GR) logs were analyzed to investigate the ST sandy horizons in the Gulf of Gabes continental shelf and to assess the potential submarine freshened groundwater occurrence.

Available data include long normal resistivity (Rt), short normal resistivity (Rxo), SP and GR, which have been used to provide information on formation porosity, lithology and, where existing, pore fluid salinity. Electrical resistivity logs were used to estimate the porosity of the offshore ST horizons, which is required to identify the existence of potential traps for offshore freshened groundwater. In contrast, GR and SP logs were used to delineate the offshore ST sequence and its subunits within this sandy-sandstone layer. GR and SP logs are commonly used in hydrogeological exploration to localize sandy and clayey facies and to define aquifer confinement conditions (Jackson and Kauahikaua, 1987; Asquith et al., 2004).

Based on the original work of Archie (1942), resistivity logs are commonly used to determine reservoir static properties, such as porosity, water saturation and saturating fluid salinity, in clay-free formations, and the logs are compared to the SP results. The water pore salinity and porosity values can be obtained from the following equation 1 (Archie, 1942).

$$F = \frac{\mathrm{Ro}}{\mathrm{Rw}} = \frac{\mathrm{Rxo}}{\mathrm{Rmf}} = a\Phi^{-m} = f^{-m} \qquad \text{(Eqn. 1)}$$

F: Formation resistivity factor.

Ro: Resistivity of the 100 % water saturated rock.

Rw: Resistivity of the fluid saturating the formation.

Rxo: Resistivity of the invaded zone.

Rmf: Resistivity of the mud filtrate.

ϕ: Porosity.

Where resistivities Ro, Rw, Rxo and Rmf are in Ω m [$ML^3T^{-3}I^{-2}$], and *a* and *m* are unitless constants related to the coefficient of saturation and the cementation factor, respectively. From an empirical study by Winsauer et al., (1952) for sandstones, *a* was determined as 0.62 and *m* as 2.15 (Humble formula), which gives the following Eqn 2 expression for the formation factor:

$$F = 0.62\Phi^{-2.15} \quad \text{(Eqn. 2)}$$

4 Results

4.1 The ST aquifer series stratigraphy and depositional environment

The ST aquifer series shows a complex stratigraphic setting, reflecting regional tectonic activity and global climatic and eustatic variations and resulting in large spatial and temporal variations of sedimentary facies (Cohen et al., 1980; Zargouni, 1985; Ben Ayed, 1986; Bédir et al., 1995). The paleogeographic reconstruction of the ST horizon has been analysed by several authors (e.g. EL Euch-EL Koundi et al., 2007; Mannaï-Tayech, 2009; Moktar and Mannaï-Tayech, 2014). Sedimentary distributions of the ST lithofacies in the Southeast Tunisian basin show a continental domain gradually migrating towards the Northwest to an open marine basin (Moktar and Mannaï-Tayech, 2014). Lithological and geochronological studies carried out to classify the geological horizons in the basin of the Gulf of Gabes showed a transition between fluvio-deltaic and lagoon fluvio-deltaic depositional environments. In the Southern onshore and offshore parts of the Gulf of Gabes basin, the ST deposits consist of the Begulia Formation, which is interpreted as a regressive sequence, and composed primarily of sand and sandstones horizons. In the Northern parts, the depositional horizons reflect a transgressive-regressive sequence of clays, sandstones and lignite intercalations (the Saouaf Formation).

The ST horizons (Begulia and/or Saouaf Formations) are water-bearing formations under confined conditions. The geometry of each aquifer system is inherited from tectonic history. Buried under the Mio-Plio-Quaternary deposits, the depth of the top of the ST varies from 30 to about 700 m. The shallowest depths are observed within the Jeffara of Gabes and the western plains of the Jeffara of Medenine: see locations Jorf and Zarzis in Fig. 14. The ST thickness, within these locations, varies between approximately 20 and 90 m with an increasing trend towards the Mediterranean Sea, and is underlain by the Senonian carbonate Formation.

The onshore Sfax region contains a larger areal extent of the ST horizons than in the Jeffara of Gabes and Jeffara of Medenine regions. Moreover, within the Sfax region, both the thicker and thinner sections of the ST horizons (Saouaf Formation) have been identified. As shown on the contour map of Figure 14c, the ST thickness gradually

360 decreases towards the NE and SW borders. The thinnest horizon (15 m) is found in the southern zone of Sfax
361 (Skhira region), where the SDA seems to meet the Gabes aquifer system. The thicker ST occupies both the western
362 border and the central part of the Sfax region. Integration of the ST depth maps (Figs. 14a, 14b) and the structural
363 configuration shows that the spatial distribution of the ST water-bearing horizons is concordant with the geological
364 structure of the region. The deepest ST deposits, in Sfax region, are encountered inside a graben where the top of
365 the ST can be found between about 700 m and 1000 m depth.
366 The presence of ST is identified in the Kerkenah archipelago and Djerba Island where it has an average thickness
367 of between about 45 m and more than 110 m (Fig.14c). Beneath these emerged Islands, ST horizons are buried
368 under younger deposits at depth between 300 m and 400 m. The thinnest and shallowest ST is detected in the South
369 West coast of Djerba Island.
370 Offshore, the ST has been identified across the entire Gulf of Gabes basin. From North to South, the ST horizon
371 is overlain and underlain, respectively, by the Melqart and Mahmoud clay-dominated formations. The ST forms a
372 confined sandy horizon of relatively uniform thickness not exceeding 315 m (Fig. 14c). The geometry of the
373 offshore ST horizons reveals an increase in depth towards the South-East. These horizons are found buried at larger
374 depths in the Ashtart basin, where they reach depths of over 1000 m (Fig. 14a). Likewise, the thickest ST horizon
375 is identified in the Ashtart basin (Fig. 14c). This geometry for the ST horizons in the basin is consistent with a
376 subsiding and faulted depositional system formed during the Middle Cretaceous (Burollet et al., 1979).
377 Based on the logs of boreholes B46, B71, B73, B76 and B77, and considering the work of Bedir (1995), a NW-
378 SE geological cross section (KL) was drawn through the basin of the Gulf of Gabes (Fig. 15). A horst and graben
379 structure were identified, showing an increase of both thickness and burial depth of ST in the Ashtart syncline
380 basin as a response to its sedimentary architecture and subsidence history.
381

382 **4.2 Groundwater flow dynamics in the Gulf of Gabes deep aquifers**

383 **4.2.1 Hydrodynamic parameters**

384 The SDA, the STG and the STZ show similarity in hydraulic conductivity and transmissivity values.
385 Transmissivity and hydraulic conductivity exhibit a wide range of values across the aquifer systems of the Gulf of
386 Gabes regions (Fig.16). Independently, each aquifer system material is permeable enough to allow groundwater
387 flow from one aquifer to another and, specifically towards, through and from the ST aquifers.
388 The SDA has relatively uniform hydraulic conductivities ranging from 1.2×10^{-4} m s^{-1} to 6.6×10^{-4} m s^{-1}, but because
389 of large variations in thickness, transmissivities are highly variable and ranging between 1.2×10^{-4} m^2 s^{-1} and

1.3×10^{-1} m^2 s^{-1}, with an average value of about 2.1×10^{-2} m^2 s^{-1}. Hydraulic conductivity values in the Gabes aquifer system generally vary from 7.5×10^{-5} m s^{-1} to 8.1×10^{-3} m s^{-1}. The Se water-bearing limestone horizon is characterized by open water-saturated fractures. The pumping tests provided transmissivity values between 0.9×10^{-3} and 3.5×10^{-1} m^2 s^{-1} (Mamou, 1990). The Tu water-bearing horizon, which is also characterized by a dual-porosity, exhibits high transmissivities, with arithmetic mean values of about 1.0×10^{-1} m^2 s^{-1} (Rouatbi, 1967). The STG is characterized by transmissivity values ranging from 3.0×10^{-3} to 3.4×10^{-2} m^2 s^{-1} (Mekrazi, 1975). Hydraulic conductivity values in the J aquifer vary from 1×10^{-5} m.s^{-1} to 8.7×10^{-4} m.s^{-1} and the transmissivity values are between 5.5×10^{-4} m^2 s^{-1} and 2×10^{-2} m^2 s^{-1}. The estimated transmissivity value in the STZ is 3.4×10^{-2} m^2 s^{-1}, and the hydraulic conductivity between 1.0×10^{-4} m s^{-1} and 5.0×10^{-4} m s^{-1}.

4.2.2. Piezometry

The 2018 piezometric maps of the aquifer systems (SDA, STG and STZ) are presented in figure 17. The piezometric map indicates that groundwater flows from the aquifer's recharge zones, i.e. lateral inflow from the neighboring aquifers for SDA, STG and STZ, towards the offshore extension in the Mediterranean Sea. Piezometric levels in the Southern zones (South of Gabes and Medenine regions) are relatively higher than in the Northern ones (Sfax and North of Gabes regions) as they are receiving water from the CI mega aquifer. Groundwater in each region flows independently towards the Mediterranean Sea direction, and they are locally abstracted in Kerkenah archipelago (Sfax region) and Djerba Island (Medenine region). Groundwater flows are driven by hydraulic gradients which have an average value of about 0.09 m/km in the SDA, 4.2 m/km in the Gabes aquifer system and about 1 m/km in the Medenine Aquifer system.

In more detail across the regions, the general groundwater flow direction in the SDA in the Sfax basin is from the North-West to the South-East, whereas it is from South-West to North-East in the North of Gabes and the Medenine basins. The piezometric levels in the SDA decrease gradually from 49 m to 25 m towards the sea, compared to 39 m to 22 m in the North of Gabes basin, and from 43 m to 21 m in the Medenine basin. At the Northern and Southern edges of the SDA, significant drawdowns in groundwater levels are observed, probably related to intensive exploitation in these areas.

4.3 Wireline logging data

The Electrical resistivity, SP and GR logs, penetrated the ST reservoir layers to the following thickness: 325 m, 205 m and 350 m in B71, 239 m, 256 m and 319 m in B74 and 317 m, 257 m and 377 m in B75. The response of

the natural GR and SP (Fig. 18) shows three different log curve shapes. Analysis of the GR and SP records clearly show that the ST horizons are sealed by significantly thick impermeable clay layers. The upper and lower boundaries of the ST horizon were found at depths of 789 m and 1104 m for B71, 796 m and 1052 m for B74, and 869 m and 1126 m for B75, respectively. Likewise, GR and SP curves indicate a dominant sand fraction for the ST deposits. Detailed analysis of the log curve shape, at this horizon, indicates the presence of significant clean sand and sandstone with slight intercalations of thin clayey sand beds.

Assessment of freshwater in sandy zones of the ST was done through the comparison of GR, SP and resistivity logs. The resistivity measurements of both the long normal resistivity (Rt) log and the short normal resistivity (Rxo) are usually greater in the ST than values measured in the Melqart and Mahmoud impermeable formations and reflect the ST rocks' water content. The resistivity logs analysis shows that resistivity increases rapidly in clayey sand intercalations. Increasing the ratio of clay to water pore content could reasonably lead to an increase in electrical resistivity.

The NaCl-salinity is calculated using a salinity–resistivity (Rw) chart at standard formation temperature (Schlumberger, 1959). The formation-water resistivity (Rw) is obtained, according to the Archie equation, from Ro, Rxo and Rmf. The NaCl-salinity of the ST water-bearing horizon yielded values for interstitial waters of between 5.5 g/L and 7.5 g/L (Tab.1). Relatively low resistivity and high NaCl levels (22 g/L) were observed in the layers L2 and L3 of B75. In all probability, this is due to the presence of evaporitic beds, as described in the lithostratigraphic log of the well B75. Moreover, in front of the ST sandy horizons, the SP curve exhibits right-sided positive deflections from the shale baseline, highly evident in L1 and L4 of B75 borehole. These positive deflections indicate a formation water with salinities lower than those of the drilling mud filtrate (15-25 g/L NaCl TDS-equivalent), providing an initial clue to the existence of potential offshore freshwater groundwater bodies (Quiroga et al., 2023).

Likewise, porosity values are calculated using a formation factor–porosity chart (Schlumberger, 1959). This chart helps to quickly solve the Humble empirical equation (Eq. 2). The determination of the formation factor is a function of Ro and Rw (Archie's Law). Correlation results show high porosity values of the offshore ST horizons, ranging between 30 % and 38 % (Table 1).

Table 1 Porosity of the Serravallian-Tortonian (ST) reservoir layers and water salinity calculated from electrical resistivity data.

Borehole	Layer	Rxo (Ohm m)	Rt (Ohm m)	Rw (Ohm m)	Porosity (%)	Salinity (g/L)
B71	L1	0.8	0.6	0.75	32	7.5
	L2	0.9	0.8	0.9	30	6
B74	L1	1	0.8	1	32	5.6
	L2	0.75	0.6	1	38	5.6
	L3	1	0.9	1	30	5.6
B75	L1	1.2	0.5	0.8	36	7
	L2	0.85	0.12	0.28	-	22
	L3	0.85	0.12	0.28	-	22
	L4	1.2	0.5	0.8	36	7

5 Discussion

The Gulf of Gabes continental shelf has not been the subject of hydrogeological exploration or analysis to date. Characterization of the present offshore aquifers, which involved synthesis of lithological, structural and hydrological properties (mostly from oil & gas exploration studies), shows similarity with the offshore freshened groundwater bodies found elsewhere worldwide.

The most offshore extended aquifer in the study region is composed of siliciclastic material of ST age, sealed by impervious marl and clay. This aquifer's recharge is mainly ensured by lateral inflow from neighbouring aquifers. Figure 19 shows the thickness, salinity and porosity values of the studied aquifers (SDA, Gabes aquifer system and Medenine aquifer system) in the onshore and offshore parts. Compared to results from previous international research, the findings from the present work are consistent with other worldwide examples of offshore aquifers (Gustafson et al., 2019, Lofi et al., 2013a, Lofi et al., 2013b, Varma and Michael, 2012, Laurent, 1993).

From the previous research worldwide, case study examples include the United States continental shelf, specifically the New Jersey offshore freshened aquifer. That case is relevant to the present study, as the aquifers are made of siliciclastic materials of Miocene age and capped at the top and the bottom by low-permeability clay acting as confining boundary layers (Gustafson et al., 2019). Also, groundwater in the South-Eastern Australian continental shelf has been found within confined sediments that show similar lithological composition in both the terrestrial and marine sides (Glenton 1983; Kuttan et al., 1986). In the North-Western Mediterranean basin, fresh to brackish water bodies, underlain by saline water, were discovered beneath the seabed on the Gulf of Lions

continental shelf (Lofi et al., 2013b). Earlier examples of offshore freshened groundwater aquifers were discovered in the continents of America, Australia and Europe, where the offshore water is derived from recent meteoric water via an active present-day onshore-offshore transport mechanism. Identification of these offshore aquifers and their structures has been carried out by using similar geological and geophysical methods as presented in this work.

This research provides evidence that extensive offshore freshened groundwater resources exist in Tunisia and likely elsewhere in the Southern Mediterranean coast with a similar geological setting. In Gabes, the offshore aquifers are already exploited for water supply in Kerkenah and Djerba Islands, which are an emerged extension of the Gulf of Gabes continental shelf.

Already operational groundwater desalination plants in Kerkenah, Gabes and Djerba may also use these freshened groundwater resources through new offshore water wells. More elaborate socioeconomic projects that make use of this resource, like ecotourism islands, green farming and so on, are also possible.

6 CONCLUSIONS

The combination of geological, geophysical and hydrogeological analyses provides solid evidence for the existence of freshened offshore groundwater stored in confined material beneath the Gulf of Gabes, Tunisia.

Over the coastal region of the Gulf of Gabes, the hydrogeological structure of the deep confined aquifers and the groundwater occurrence are relatively simple. The main aquifer is found in confined ST sandy horizons which have variable thickness and depth, and a general dip towards the sea. Regional mapping of water heads shows high potentiometric surfaces, providing positive vertical hydraulic gradients with seaward flow directions. The water budget (as inflows minus pumping abstraction) indicates a residual outflow term, assumed to support submarine groundwater discharge SGD. Analysis of the estimated total inflows to the SDA, Gabes aquifer system and Medenine aquifer system (i.e. aquifer recharge rates) and the outflows (i.e. discharge to the sea and groundwater pumping) show inconsistent data. Hence, the use of numerical models is needed to improve understanding of the aquifer systems and better quantify the water budget components.

The spatial distribution of the lithostratigraphic horizons suggests continuity between the onshore and offshore parts. Offshore, the ST horizons are identified across the entire Gulf of Gabes basin. The sandy horizons extend seaward with porous and permeable sediments, making a good aquifer with a confined sandy horizon of a porosity over 30 % and an average thickness of 200 m. This aquifer is sealed by the thick confining beds of the Melqart Formation at its top and of the Mahmoud Formation at its base. Groundwater NaCl-salinity values, obtained from

borehole resistivity measurements, range from about 5.5 g/L to 7.5 g/L, which are in the same range as salinity values observed in the onshore part of the aquifer system. The offshore freshened groundwater beneath the Gulf of Gabes can be extracted via existing hydrocarbon infrastructures.

Further detailed and integrated studies are necessary to precisely delineate the freshened offshore groundwater bodies and estimate more accurately the reservoir water storage and balance using numerical modeling techniques.

Conflict of interest

On behalf of all authors, the corresponding author states that there is no conflict of interest.

REFERENCES

Abid, K., Zouari, K., Dulinski, M., Chkir, N., Abidi, B., 2011. Hydrologic and geologic factors controlling groundwater geochemistry in the Turonian aquifer (southern Tunisia). Hydrogeology Journal,19, 415-427, DOI: 10.1007/s10040-010-0668-z.

Abid, K., Hadj Ammar, F., Chkir, N., Zouari, K., 2012. Relationship between Senonian and deep aquifers in Southern Tunisia, Quaternary International, 257, 13-26, DOI: 10.1016/j.quaint.2011.09.022.

Abidi, B., 2001. La nappe du Continental Intercalaire du Sud-Est Tunisien : Analyse de la situation actuelle (The Continental Intercalary aquifer in South East Tunisia : Analysis of the actual situation), report. DGRE (General Directorate of Water Resources) Tunisia 2001, 228 p.

Abidi, B. 2004. Caractéristique hydrodynamique et Géochimique de la Djeffara de Gabès (Hydrodynamic and geochemical characteristics of the Djeffara of Gabes), report. DGRE (General Directorate of Water Resources) Tunisia 2004, 120 p.

Archie, G. E, 1942. The Electrical Resistivity Log as an Aid in Determining Some Reservoir Characteristics. Petroleum Transactions of the AIME, 146, pp. 54-62.

Arroyo, J., Shirazi, S., 2012. Cost of brackish groundwater desalination in Texas, Texas Water Development Board.

Asquith, G.B., Krygowski, D. and Gibson, C.R., 2004. Basic well log analysis (Vol. 16). Tulsa: American Association of Petroleum Geologists.

Ayenew, T., Demlie, M., Wohnlich, S., 2008. Hydrogeological framework and occurrence of groundwater in the Ethiopian aquifers. Journal of African Earth Sciences, 52(3): 97-113.

Bachtouli, S., Comte, J-C., 2019. Regional-scale analysis of the effect of managed aquifer recharge on saltwater intrusion in irrigated coastal aquifers: long-term groundwater observations and model simulations in NE Tunisia. Journal of Coastal Research, 35(1): 91-110, DOI: 10.2112/JCOASTRES-D-17-00174.1.

Bakker, M., 2006. Analytic solutions for interface flow in combined confined and semi-confined, coastal aquifers. Advances in Water Resources, 29(3): 417-425, DOI: 10.1016/j.advwatres.2005.05.009.

Bédir, M., 1995. Mécanismes géodynamiques des bassins associes aux couloirs de coulissement de la marge Atlasique de la Tunisie. Seismo-stratigraphie, seismo-tectonique et implications pétrolières. (Geodynamic mechanisms of the basins associated with the sliding corridors of the Atlas margin of Tunisia. Seismo-stratigraphy, seismo-tectonics and petroleum implications). Doctorate es Science. University of Tunis II, Tunisia, 407 p.

Ben Ayed, N., 1986. Evolution tectonique de l'avant-pays de la chaîne alpine de Tunisie du début du Mésozoïque à l'Actuel (Tectonic evolution of the foreland of the Tunisian Alpine chain from the early Mesozoic to the actual). Doctorate es Science. University of Paris-11, France.

Ben Baccar, B., 1982. Contribution à l'étude hydrogéologique de l'aquifère multicouche de Gabès-Sud. (Contribution to the hydrogeological study of the Gabès-Sud multilayer aquifer). Doctorate Thesis. University of Paris South (Orsay Central), 113 p.

B. Ferjani, A. Burollet, P.F., Mejri, F., 1990. Petroleum geology of Tunisia. Entreprise Tunisienne d'Activités Pétrolière (ETAP), Memoire Ed, p.194.

Ben Jemaa, F., Houcine, I., Chahbani M.H., 1998. Desalination in Tunisia: Past experience and future prospects. Desalination, 116(2-3): 123-133, DOI:10.1016/S0011-9164(98)00189-1.

Ben Othman, S., 1973. Le Sud tunisien (golfe de Gabès) : hydrologie, sédimentologie, flore et faune. (The Tunisian South (Gulf of Gabes): hydrology, sedimentology, flora and fauna). Doctorate Thesis, University of Sciences Tunis, Tunisia, 166 p.

Benton, M.J., Bouaziz, S., Buffetaut, E., Martill, D., Ouaja, M., Soussi, M., Trueman, C.N., 2000. Dinosaurs and other fossil vertebrates from fluvial deposits in the Lower Cretaceous of southern Tunisia. Paleogeography, Paleoclimatology, Paleoecology, V. 157, pp 217-231.

Bertoni, C., Lofi, J., Micallef, A., Moe, H., 2020. Seismic reflection methods in offshore groundwater research. Geosciences, 10(8), 299, DOI: 10.3390/geosciences10080299

Biely, A., Rakus, M., Robinson, P., Salaj, J., 1972. Essai de corrélation des formations Miocènes au Sud de la Dorsale Tunisienne (Attempt of Miocene formations correlation in south of the Tunisian Dorsal). Notes Services géologique Tunisia, vol. 38, pp 73-92.

Boretti, A., Rosa, L. (2019) Reassessing the projections of the World Water Development Report. npj Clean Water 2, 15. https://doi.org/10.1038/s41545-019-0039-9.

559 Borghini, M., Bryden, H., Schroeder, K., Sparnocchia, S., Vetrano, A., 2014. The Mediterranean is becoming saltier.
560 Ocean Science Journal, 10, 693-700, DOI: 10.5194/os-10-693-2014.
561 Bouaziz, S., 1995. Etude de la tectonique cassante dans la plateforme et l'Atlas sahariens (Tunisie méridionale) :
562 évolution des paléo-champs de contraintes et implications géodynamiques. (Study of brittle tectonics in the
563 Saharan platform and Atlas (southern Tunisia): evolution of stress paleofields and geodynamic implications).
564 Doctorate es Science. University of Tunis II, Tunisia, 485 p.
565 Bouaziz, S., Barrier, E., Soussi, M.M., Turki, M.M., Zouari, H., 2002. Tectonic evolution of the northern African
566 margin in Tunisia from paleostress data and sedimentary record. Tectonophysics 357, 227-253, DOI:
567 10.1016/S0040□1951(02)00370□0.
568 Bouri, S., Ben Dhia, H., 2010. A thirty-year artificial recharge experiment in a coastal aquifer in an arid zone: The
569 Teboulba aquifer system (Tunisian Sahel). Comptes Rendus Geosciences, 342 (1): 60-74, DOI:
570 10.1016/j.crte.2009.10.008.
571 Bratton, J.F., 2007. The importance of shallow confining units to submarine groundwater flow. IAHS-AISH
572 Publication, 312, 28-34.
573 Brown, K.M., Saffer, D.M., Bekins, B.A., 2001. Smectite diagenesis, pore-water freshening, and fluid flow at the
574 toe of the Nankai wedge. Earth and Planetary Science Letters, 194(1-2): 97-109, DOI: 10.1016/S0012-821X
575 (01)00546-5.
576 Burollet, P.F., 1956. Contribution à l'étude stratigraphique de la Tunisie centrale. (Contribution to the stratigraphic
577 study of central Tunisia). Annales des Mines et de la Géologie (Tunisia), vol. 18, 350 p.
578 Burollet, P.F., Winnock. E., Templeton. R.S.M., Desprat. R.B., 1979. Essai de synthèse : La mer pélagienne. Etude
579 sédimentologique et écologique du Plateau tunisien et du Golfe de Gabès. (Tentative of synthesis: The Pelagic Sea.
580 Sedimentological and Ecological Study of the Tunisian Plateau and the Gulf of Gabes) Mediterranean Geology
581 Tome 6, N° 1, 1979.pp. 321-328, DOI: 10.3406/geolm.1979.1097.
582 Busson, G., 1967. Mesozoic of southern Tunisia, In Ninth Annual field conference of Petroleum. Exploration
583 Society of Libya, 1967, pp 131-152.
584 Castany, G., 1951. Etude géologique de l'Atlas tunisien oriental. (Geological study of the Tunisian Oriental Atlas).
585 Annales Mines et Géologie, Tunis, nº 8, Volume 4, PhD Thesis Es-Sc., Paris, France, 632 p.
586 Castany, G., 1954. L'accident sud-tunisien, son âge et ses relations avec l'accident sud-atlasique d'Algérie (The
587 South Tunisian accident, its age and its relationship with the South Atlas accident in Algeria). Comptes Rendus de
588 l'Académie des Sciences, Paris, France, 238, pp 916-918.

589 Clark, P.U., Dyke, A.S., Shakun, J.D., Carlson, A.E., Clark, J., Wohlfarth, B., Mitrovica, J.X., Hostetler, S.W.,
590 McCabe, A.M., 2009. The Last Glacial Maximum. Science, 325(5941): 710-4, DOI: 10.1126/science.1172873.
591 Cobbing, J., Hiller, B., 2019. Waking a sleeping giant: Realizing the potential of groundwater in Sub-Saharan
592 Africa. World Development, 122, 597-613, DOI: 10.1016/j.worlddev.2019.06.024.
593 Cohen, C.R., Schamel, S., Boyd Kaygi, P., 1980. Neogene deformation in Northern Tunisia: origin of the eastern
594 Atlas by microplate-continental collision. Geological Society of America Bulletin 91(4): 225–237.
595 CRDA Sfax, 2005. Programme intégré pour la mise en place en valeur des régions du Sahara et du Sud de la
596 Tunisie, Lot°8, Etude des nappes aquifères de Sfax (Integrated program for the development of the regions of the
597 Sahara and the South of Tunisia, Lot°8, Study of the aquifers of Sfax), Report, Regional Agricultural Development
598 Office of Sfax, Tunisia
599 Custodio, E., Bruggeman, G.A., 1987. Groundwater problems in coastal areas: a contribution to the International
600 Hydrological Programme. Studies and reports in Hydrology. Paris: UNESCO.
601 DGRE, 2018 a. Annuaire de l'exploitation des nappes profondes (Yearbook of deep aquifer exploitation 2018,
602 Tunisia). General Directorate of Water Resources
603 DGRE, 2018 b. Annuaire piézométrique de la Tunisie (Yearbook of piezometry of Tunisia 2018). General
604 Directorate of Water Resources
605 Domenico, P.A., Schwartz, F.W., 1990. Physical and chemical hydrogeology. Wiley, New York, pp 410-420.
606 Dona, N.C., Hangb, N.T.M, Arakia, H., Yamanishia, H., Kogac, K., 2006. Groundwater resources and management
607 for paddy field irrigation and associated environmnetal problems in an alluvial coastal lowland plain. Agricultural
608 Water Mangement, 84 (3): 295-304, DOI: 10.1016/j.agwat.2006.03.006.
609 Edmunds, W.M., Guendouz, A., Mamou, A., Moulla, A., Shand, P., Zouari, K., 2003. Groundwater evolution in
610 the Continental Intercalaire aquifer of the Southern Algeria and Tunisia: trace element and isotopic indicators.
611 Applied Geochemistry, 18(6): 805-822, DOI: 10.1016/S0883-2927(02)00189-0.
612 EL Euch-EL Koundi, N., Fery, S., Ouja, M., Ben Salem H., Zargouni, F., 2007. Sédimentologie et stratigraphie
613 séquentielle de série miocène moyenne de cap bon, Tunisie nord-orientale. (Sedimentology and sequence
614 stratigraphy of the Middle Miocene series of Cap Bon, north-eastern Tunisia) Note du service géologique de la
615 Tunisie, n°75, 53-6, Tunisia.
616 Golden Software, 2014, SURFER Version 12: Reference Manual, Golden Software, Inc., Golden, Colorado, U.S.A,
617 2014.

618 Guler, C., Thyne, G.D., 2004. Hydrologic and geologic factors controlling surface and groundwater chemistry in
619 Indian Wells-Owens Valley area, Southeastern California, USA. Hydrogeology Journal, 285, 177-198, DOI:
620 10.1016/j.jhydrol.2003.08.019.
621 Gustafson, C., Key, K., Evans, R.L., 2019. Aquifer systems extending far offshore on the U.S. Atlantic margin.
622 Scientific Reports, 9, 8709, DOI: 10.1038/s41598-019-44611-7.
623 Hamzaoui Azaza, F.,Tlili Zrelli, B., Bouhlila, R., Gueddari, M., 2013. An integrated statistical methods and
624 modeling minerals□water interaction to identifying hydrochemical processes in groundwater in southern Tunisia.
625 Chemical Speciation and Bioavailability, 25(3): 165-178.
626 Henia, L., 1993. Climat et bilans de l'eau en Tunisie : essai de régionalisation climatique par les bilans hydriques.
627 (Climate and water balance in Tunisia: test of climatic regionalisation by water balances). University of Tunis
628 Publication, Tunisia, 391 p.
629 Hensen, C., Wallmann, K., Schmidt, M., Ranero, C.R., Suess, E., 2004. Fluid expulsion related to mud extrusion
630 off Costa Rica-A window to the subducting slab. Geology, 32(3): 201-204, DOI: 10.1130/G20119.1.
631 Hong, W.L., Lepland, A., Himmler, T., Kim, J.H., Chand, S., Sahy, D., Solomon, E.A., Rae, J.W.B., Martma, T.,
632 Nam, S-II, Knies, J., 2019. Discharge of Meteoric Water in the Eastern Norwegian Sea since the Last Glacial
633 Period. Geophysical Research Letters, 46(14): 8194-8204, DOI: 10.1029/2019GL084237.
634 Jackson, D., Kauahikaua, J., 1987. Regional self-potential anomalies at Kilauea Volcano. Volcanism in Hawaii.
635 U.S.G.S. Prof. Paper 1350, 947–959 (Chapter 40).
636 Jouet, G., Berné, S., Rabineau, M., Bassetti, M..A., Bernier, P., Dennielou, B., Sierro, F.J., Flores, J.A., Taviani,
637 M., 2006. Shoreface migrations at the shelf edge and sea-level changes around the Last Glacial Maximum (Gulf
638 of Lions, NW Mediterranean). Marine Geology, 234(1-4): 21-42, DOI: 10.1016/j.margeo.2006.09.012.
639 Kamel, S., Dassi, L., Zouari, K., 2006. Hydrogeological and hydrochemical approach of hydrodynamic exchanges
640 between deep and superficial aquifers of the Djérid basin, Tunisia. Hydrological Sciences Journal, 51(4): 713-730.
641 Kammoun, M.A., Gassara, S., Palmeri, J., Ben Amar, R., Deratani, A., 2020. Nanofiltration performance prediction
642 for brackish water desalination: case study of Tunisian groundwater. Desalination and Water Treatment, 181: 27-
643 39, DOI: 10.5004/dwt.2020.25100.
644 Kastner, M., Elderfield, H., Martin, J., Suess, E., Kvenvolden, K., Garrison, R., 1990. Diagenesis and interstitial-
645 water chemistry at the Peruvian continental margin; major constituents and strontium isotopes. Proc. Ocean Drill.
646 Program 112, 413-440, DOI: 10.2973/odp.proc.sr.112.144.1990.

Kingumbi, A., Bergaoui, Z., Bourges, J., Hubert, P., Kallel, R., 2001. Etude de l'évolution des séries pluviométriques de la Tunisie. Hydrologie des Régions Méditerranéennes (Study of the evolution of rainfall series in Central Tunisia). Hydrologie des Régions Méditerranéennes, actes du séminaire UNESCO-IRD, 51, 341-345.

Krijgsman, W., Hilgen, F., Raffi, I., Sierro, F.J., Wilson, D.S., 1999. Chronology, causes and progression of the Messinian salinity crisis. Nature, 400, 652-655, DOI: 10.1038/23231.

Knight, A.C., Werner, A.D., Morgan, L.K., 2018. The onshore influence of offshore fresh groundwater, Journal of Hydrology, 561, DOI: 10.1016/j.jhydrol.2018.03.028.

Kohout, F.A., 1964. The flow of fresh water and salt water in the Biscayne aquifer of the Miami area, Florida, in Sea water in coastal aquifers: Relation of salt water to fresh groundwater, edited by H. H. Cooper, et al., pp C12-33, USGS Water supply.

Kooi, H., Groen, J., 2001. Offshore continuation of coastal groundwater systems: predictions using sharp-interface approximations and variable-density flow modelling. Journal of Hydrology, 246(1-4), 19-35, DOI: 10.1016/S0022-1694(01)00354-7.

Lambeck, K., Chappell, J., 2001. Sea level change through the last glacial cycle. Science, 292(5517): 679-686, DOI: 10.1126/science.1059549.

Laurent, A., 1993. La gestion en bien commun des eaux souterraines : La nappe des sables astiens de Valras (Herault), Une opération pilote en Languedoc-Roussillon. ´PhD Thesis, Universite de Montpellier II.

Lin, I.T., Wang, C.H., You, C.F., Lin, S., Huang, K.F., Chen, Y.G., 2010. Deep submarine groundwater discharge indicated by tracers of oxygen, strontium isotopes and barium content in the Pingtung coastal zone, southern Taiwan. Marine Chemistry, 122, 51- 58, DOI: 10.1016/j.marchem.2010.08.007.

Lofi, J., Inwood, J., Proust, J.N., Monteverde, D., Loggia, D., Basile, C., Otsuka, H., Hayashi, T., Stadler, S., Mottl, M., Fehr, A., Pezard, P., 2013a. Fresh-water and salt-water distribution in passive margin sediments: Insights from Integrated Ocean Drilling Program Expedition 313 on the New Jersey Margin. Geosphere, 9 (4): 1009–1024. doi: https://doi.org/10.1130/GES00855.1

Lofi, J., Pezard, P., Bouchette, F., Raynal, O., Sabatier, P., Denchik, N., Levannier, A., Dezileau, L., Certain, R., 2013. Integrated Onshore□Offshore Investigation of a Mediterranean Layered Coastal Aquifer Groundwater, 51(4): 550–561, doi:10.1111/j.1745-6584.2012.01011.x.

Mamou, A., 1990. Caractéristiques et évaluation des ressources en eau du Sud tunisien (Characteristics and water resources evolution of Tunisian South). Es-Sc Doctorate Thesis, University of Paris-South, France, 426 p.

Mamou, A., Kassah, A., 2002. Eau et développement dans le Sud tunisien (Water and development in the Tunisian South). Cahiers du CERES, série géographique n° 23, Tunis, Tunisia, 286 p.

Mannaï-Tayech, B., 2009. The lithostratigraphy of Miocene series from Tunisia, revisited. Journal of African Earth Sciences, 54 (3-4): 53-6, DOI: 10.1016/j.jafrearsci.2009.02.003.

Manzi, V., Gennari, R., Hilgen, F., Krijgsman, W., Lugli, S., Roveri, M., Sierro, F.J., 2013. Age refinement of the Messinian salinity crisis onset in the Mediterranean. Terra Nova, 25, 315-322, DOI: 10.1111/ter.12038.

Mekrazi, A.F. 1975. Contribution à l'étude géologique et hydrogéologique de la région de Gabès Nord (Contribution to the Hydrogeological study of the Gabes North region). Es-Sc Doctorate Thesis. University of Bordeaux I, France,169 p.

Micallef, A., Berndt, C., Berndt, J., Jegen, M., Schwalenberg, K., Wollatz Vogt, M., Haroon, A., Gazia, X., Faghih, Z., Spatola, D., Worzewski, T., Zerbst, J., Marcon, 2018. Cruise Report RV Hercules [MARCAN Malta 2018], Valletta-Valletta, 1.- 10.10.2018, 37 pp, University of Malta, Malta.

Micallef, A., Person, M., Haroon, A., Weymer, B.A., Jegen, M., Schwalenberg, K., Faghih, Z., Duan, S., Cohen, D., Mountjoy, J.J., Woelz, S., Gable, C.W., Averes, T., Kumar Tiwari, A., 2020. 3D characterization and quantification of an offshore freshened groundwater system in the Canterbury Bight. Nature Communications 11(1):1372, DOI:10.1038/s41467-020-14770-7.

Micallef, A., Person, M., Berndt, C., Bertoni, C., Cohen, D., Dugan, B., et al., 2021. Offshore freshened groundwater in continental margins. Reviews of Geophysics, 59, e2020RG000706. https://doi.org/10.1029/2020RG000706.

Middelburg, J.J., de Lange, G.J., 1989. The isolation of Kau Bay during the last glaciation: direct evidence from interstitial water chlorinity. Netherlands Journal of Sea Research, 24(4): 615-622, DOI: 10.1016/0077-7579(89)90138-5.

Miller, K. G., Schmelz, W. J., Browning, J. V., Kopp, R. E., Mountain, G. S., Wright, J. D., 2020. Ancient Sea Level: as Key to the Future. Oceanography, 33(2): 32–41. https://www.jstor.org/stable/26937737. Cited 15 March 2021

Moktar, N.B., Mannaï-Tayech, B., 2014. Palynology and sedimentology of the Miocene series in the north-east of Tunisia: the climatic and eustatic signature. Arabian Journal of Geosciences, 7, 385-396, DOI: 10.1007/s12517-012-0808-y.

Moore, W.S., 2010. The effect of submarine groundwater discharge on the ocean. Annual Review of Marine Science, 2:59-88, DOI: 10.1146/annurev-marine-120308-081019.

Mora, G., 2005. Isotope-tracking of pore water freshening in the fore-arc basin of the Japan Trench. Marine Geology, 219(2-3): 71-79, DOI: 10.1016/j.margeo.2005.06.020.

Muldoon, M., Simo, J.A., and Bradbury, K.R., 2001, Correlation of hydraulic conductivity with stratigraphy in a fractured-dolomite aquifer, northeastern Wisconsin, USA: Hydrogeology Journal, 9, 570–583.

Mulligan, A., Charette, M., 2009. Groundwater Flow to the Coastal Ocean. Encyclopedia of Ocean Sciences, DOI: 10.1016/B978-012374473-9.00645-7.

OSS, 2003. Le système aquifère du Sahara septentrional. 3 vols: Hydrogéologie, Base de données et Modèle mathématique (The Northern Sahara aquifer system 3 vols: Hydrogeology, Data base of the mathematical model)., by the Sahara and Sahel Observatory (OSS), Tunisia.

OSS, 2005. Water resources and management of transboundary aquifers in North Africa and the Sahel. ISARM-AFRICA, UNESCO IHP-IV, Series on Groundwater, n11, Paris, 134 p.

OSS, 2006. Etude hydrogéologique du système aquifère de la Jeffara tuniso-libyenne (Hydrogeological study of Tunisian Libyan Jeffara aquifer), Sahara and Sahel Observatory, Tunisia internal report, 209 p.

Post, V.E.A., 2005. Fresh and saline groundwater interaction in coastal aquifers: Is our technology ready for the problems ahead? Hydrogeology Journal, 13, 120-123, DOI: 10.1007/s10040-004-0417-2.

Post, V., Groen, J., Kooi, H., Person, M., Ge, S., Edmunds, W.M., 2013. Offshore fresh groundwater reserves as a global phenomenon. Nature, 504, 71-78, DOI: 10.1038/nature12858.

Quiroga, E., Bertoni, C. & Ruden, F., 2023. Deep low-salinity groundwater in sedimentary basins: petrophysical methods from a case study in Somalia. Hydrogeol. J., 31, 685-705. https://doi.org/10.1007/s10040-022-02589-z

Ritchie H. and Roser M. (2017) Water Use and Stress. Published online at: https://ourworldindata.org/water-use-stress. Cited 12 March 2021

Robertson, F.N., 1989. Groundwater geochemistry and information transfer in alluvial basins in Arizona. In: Simpson, E.S., Sharp, J.M. (Eds.), Selected Papers on Hydrogeology. International Association of Hydrogeologists, pp 223-234.

Roederer, P., 1956. Soil permeability (Porchet method) (in Frennch). Tunis: SSEPH, (19), 12 p, multigr. (Etudes Spéciales-SSEPH; 19).

Rouatbi, R. 1967. Contribution to the hydrogeological study of the Karst in the land of South of Gabes. Doctorate Thesis, Montpellier, France 270p.

Sahli, H., Tagorti, M.A., Tlig, S., 2013. Groundwater Hydrochemistry and Mass Transfer in a Stratified Aquifer System (Jeffara-Gabès Basin, Tunisia). Larhyss Journal, 10, 95-108.

736 Sanchez-Vila, X., Guadagnini, A., Carrera, J., 2006. Representative hydraulic conductivities in saturated
737 groundwater flow. Reviews of Geophysics, 44 (3): 8755-1209, DOI: 10.1029/2005RG000169.
738 Shanmugam, G., 2012. Chapter 5-Initiation of Deep-Water Sediment Failures. Handbook of Petroleum
739 Exploration and Production 9 221-270, DOI:10.1016B978-0-444-56335-4.00005-9.
740 Shirazi, S., Imran, H.M., Akib, S., Yusop, Z., Harun, Z., 2013. Groundwater vulnerability assessment in the Melaka
741 State of Malaysia using DRASTIC and GIS techniques. Environmental earth sciences, 70(5), DOI:
742 10.1007/s12665-013-2360-9.
743 Southgate, H.N., Möller, N.K., 2000. Fractal properties of coastal profile evolution at Duck, North Carolina.
744 Journal of Geophysical Research, 105(C5): 11489-11507, DOI: 10.1029/2000JC900021.
745 Tayfur, G., Nadiri, A.A., Moghaddam, A.A., 2014. Supervised Intelligent Committee Machine Method for
746 Hydraulic Conductivity Estimation. Water Resources Management, 28, 1173-1184, DOI: 10.1007/s11269-014-
747 0553-y.
748 Thomas, A.T., Reiche, S., Riedel, M., Clauser, C., 2019. The fate of submarine fresh groundwater reservoirs at the
749 New Jersey shelf, USA. Hydrogeol. J 27, 2673–2694. https://doi.org/10.1007/s10040-019-01997-y
750 Trabelsi, R., 2009. Caractérisation hydrogéologique et géochimique du système aquifère de la Djeffara, sud-est
751 tunisien : modélisation et intrusion marine (Hydrogeological and geochemical characterization of the Djeffara
752 aquifer system, South-East Tunisia : Modeling and marine intrusion). Doctorate Thesis. National Engineering
753 School of Sfax (ENIS), Tunisia, 235 p.
754 Trabelsi, R, Zairi, M, Ben Dhia, H., 2007. Groundwater salinization of the Sfax super*fi*cial aquifer, Tunisia
755 Hydrogeology Journal, 15: 1341–1355. DOI 10.1007/s10040-007-0182-0
756 Tramblay, Y., Ruelland, D., Hanich, L., & Dakhlaoui, H. 2016. Sub-chapter 2.3.1. Hydrological impacts of climate
757 change in North African countries. In Moatti, J., & Thiébault, S. (Eds.), The Mediterranean region under climate
758 change: A scientific update. IRD Éditions. doi:10.4000/books.irdeditions.23496.
759 Varma, S., Michael, K., 2012. Impact of multi-purpose aquifer utilization on a variable-density groundwater flow
760 system in the Gippsland Basin, Australia. Hydrogeology Journal, 20, 119–34.
761 Water Reuse Association (WRA), 2012. Seawater Desalination Costs, January 2012.
762 Weymer, B.A., Wernette, P.A., Everett, M.E., Pondthai, P., Jegen, M., Micallef, A., 2020. Multi-Layered High
763 Permeability Conduits Connecting Onshore and Offshore Coastal Aquifers. Frontiers in Marine Science, 7, 903,
764 DOI: 10.3389/fmars.2020.531293.

765 Williams, J.H., Lane, J.W., Singha, K., Haeni, F.P., 2002. Application of advanced geophysical logging methods
766 in the characterization of a fractured-sedimentary bedrock aquifer, Ventura County, California: U.S. Geological
767 Survey Water-Resources Investigations Report 00-4083. 28 pp.
768 Winsauer, W.O., Shearin, H.M., Masson, P.H., Williams, M.,1952. Resistivity of brine-saturated sands in relation
769 to pore geometry. American Association of Petroleum Geologists Bulletin, Vol. 36, No. 2, 1952, pp. 253- 277.
770 Xiao, H., Wang, D., Medeiros, S.C., Hagen, S.C., Hall, C.R., 2018. Assessing sea-level rise impact on saltwater
771 intrusion into the root zone of a geo-typical area in coastal east-central Florida. Science of The Total Environment,
772 630, 211-221, DOI: 10.1016/j.scitotenv.2018.02.184.
773 Zamrsky, D., Karssenberg, M.E., Cohen, K.M., Bierkens, M.F.P., Oude Essink, G.H.P., 2020. Geological
774 Heterogeneity of Coastal Unconsolidated Groundwater Systems Worldwide and Its Influence on Offshore Fresh
775 Groundwater Occurrence. Frontiers in Earth Science, 7(339), DOI: 10.3389/feart.2019.00339.
776 Zargouni, F., 1985. Tectonique de l'Atlas méridional de Tunisie, évolution géométrique et cinematique des
777 structures en zone de cisaillement (Tectonics of the Southern Atlas of Tunisia, geometric and kinematic evolution
778 of structures in shear zone). Doctorate Es- Sc., University of Louis Pasteur Strasbourg, France. 304 p.
779

FIGURE CAPTIONS:

Fig. 1 Location of the deep confined aquifers and main structural features of the Gulf of Gabes (SDA: Sfax deep aquifer, STG: Serravallian-Tortonian aquifer of Gabes region, STZ: Serravallian-Tortonian aquifer of Medenine region, Se: Senonian aquifer, Tu: Turonian aquifer, J: Jurassic aquifer, T: Triassic aquifer.

Fig. 2 Lithostratigraphic log for the Cretaceous to Quaternary formations in the Gulf of Gabes.

Fig. 3 General simplified schematic representation of the SDA (AB cross-section on figure 1).

Fig. 4 Geological cross-sections (**a**) NE-SW and (**b**) NW-SE (modified from CRDA Sfax, 2005, see figure 1 for cross sections location). Z = elevation in meters relative to sea level

Fig. 5 SDA exploitation evolution for the period 1980 to 2018.

Fig. 6 Groundwater depth evolution for the period 2001-2018 in the SDA.

Fig. 7 Annual lateral inflow, abstraction rate, submarine groundwater discharge (SGD) and groundwater salinity in the SDA.

Fig. 8 Geological cross-section through the Jeffara of Gabes (modified from Abidi, 2001; see figure 1 for cross section locations).

Fig. 9 Annual lateral inflow, abstraction rate, SGD and groundwater salinity ranges in the Gabes aquifer system.

Fig. 10: Groundwater depth evolution for the period 2005 and 2017 in the STG.

Fig. 11 NE-SW geological cross-section (modified from Ben Baccar, 1982; see figure 1 for location).

Fig. 12 Annual lateral inflow, abstraction rate, SGD and groundwater salinity in the Medenine aquifer system.

Fig. 13 Groundwater depth evolution for the period 1999 and 2018 in the STZ.

Fig. 14 Contour maps of the (a) depth of the top, (b) depth of the base, and (c) thickness of the Serravallian-Tortonian (ST) horizon in the Gulf of Gabes. (On-shore extension of ST horizon in yellow color).

Fig. 15 Offshore geological cross-section through the Gulf of Gabes (see Fig.1 for location).

Fig. 16 Transmissivity and hydraulic conductivity ranges in the Gulf of Gabes aquifers systems.

Fig. 17: Piezometric maps for (**a**) the Gulf of Gabes aquifers systems: SDA, J, Tu, Se, STG, T, J and STZ; and (**b)** ST aquifer level.

Fig. 18 Resistivity, SP and GR logs for boreholes B71, B74 and B75.

Fig. 19 Onshore-offshore comparison of aquifer thickness, salinity and porosity for the (a) SDA, (b) Gabes aquifer system and (c) Medenine aquifer system.

Figure 1

Click here to access/download;Figure;Figure_1.tiff

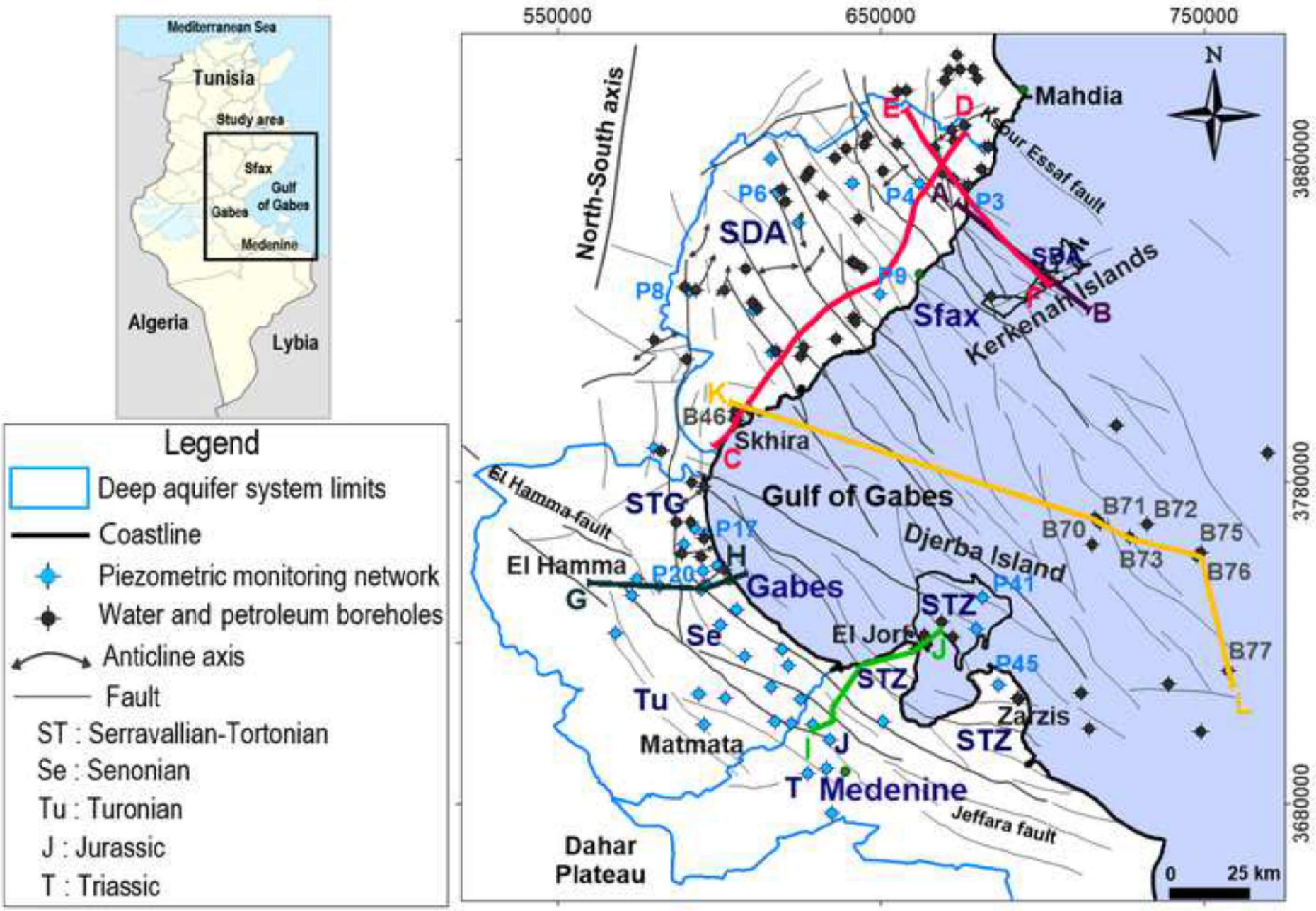

Figure 2

Click here to access/download;Figure;Figure_2.tiff

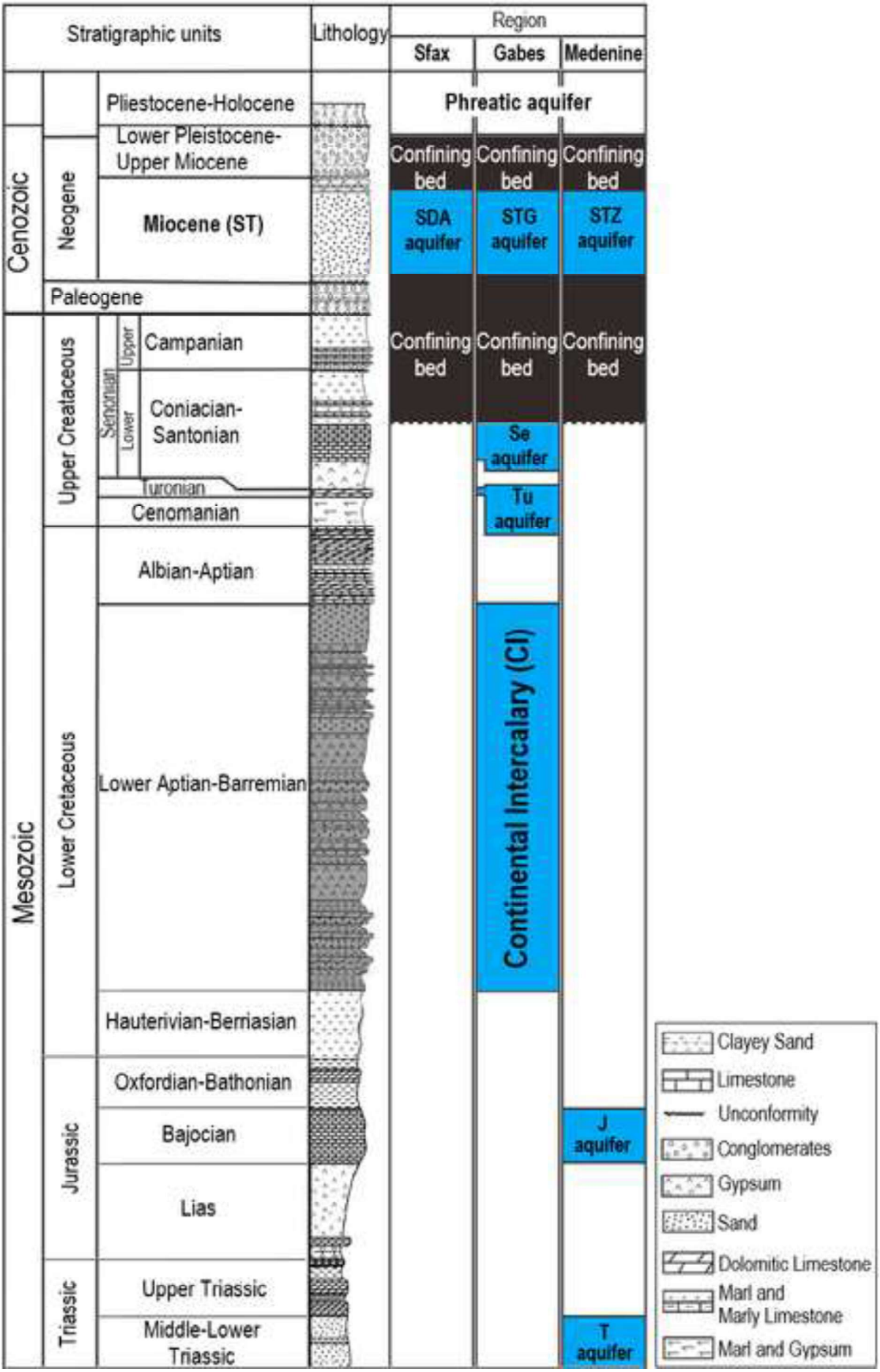

Figure 3

Click here to access/download;Figure;Figure_3.tif

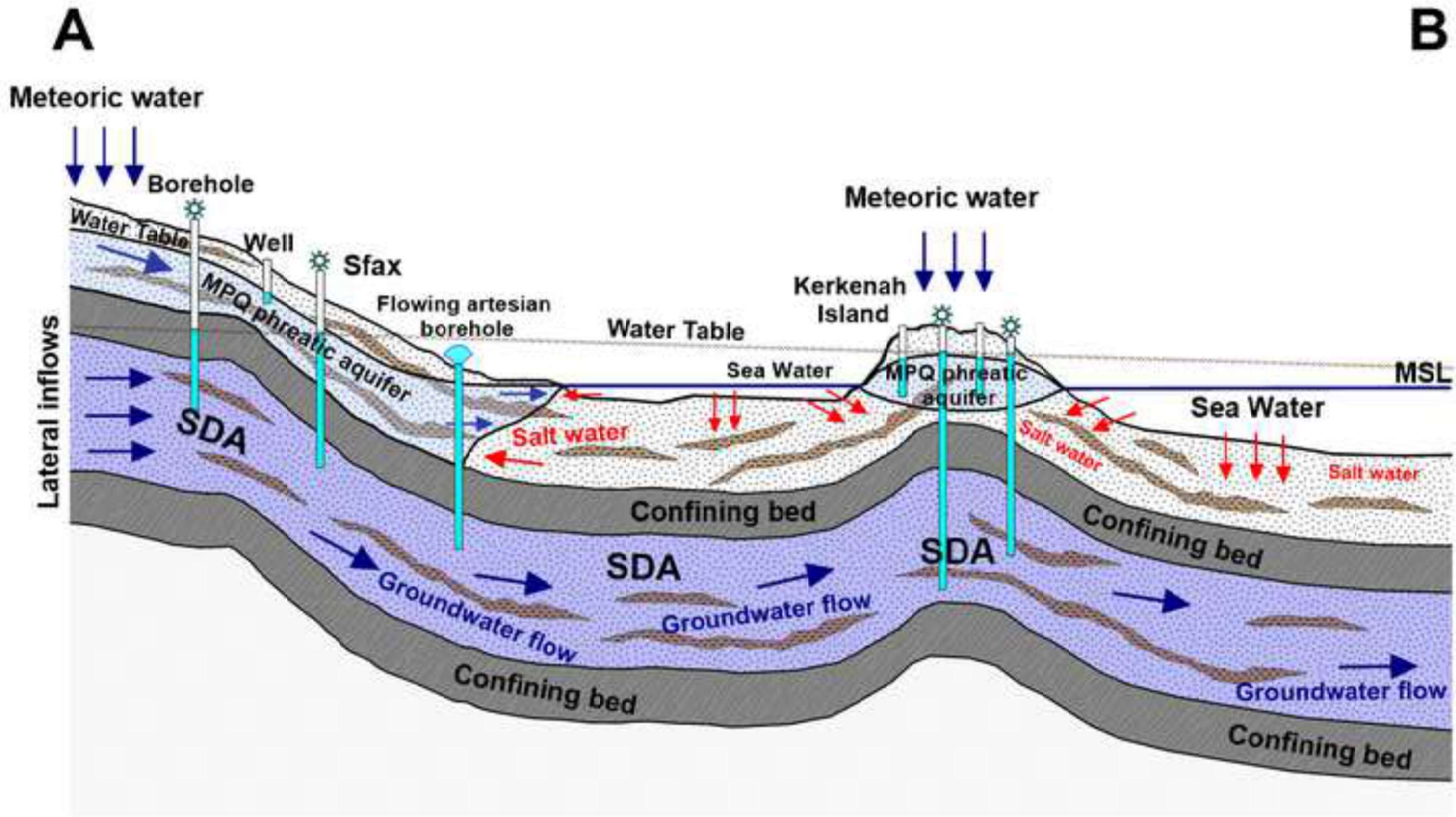

Figure 4

Click here to access/download;Figure;Figure_4.tiff

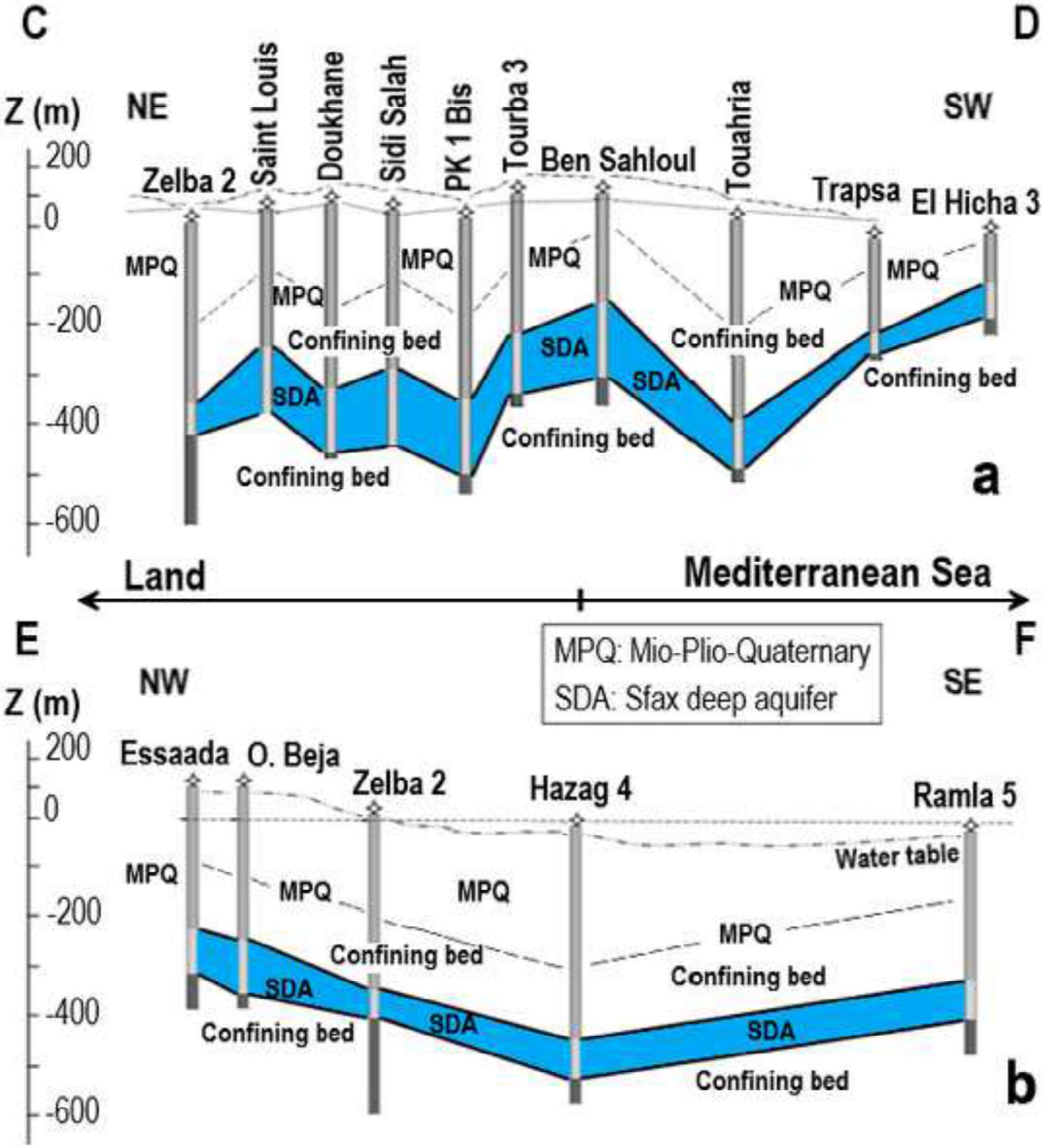

Figure 5

Click here to access/download;Figure;Figure_5.tiff

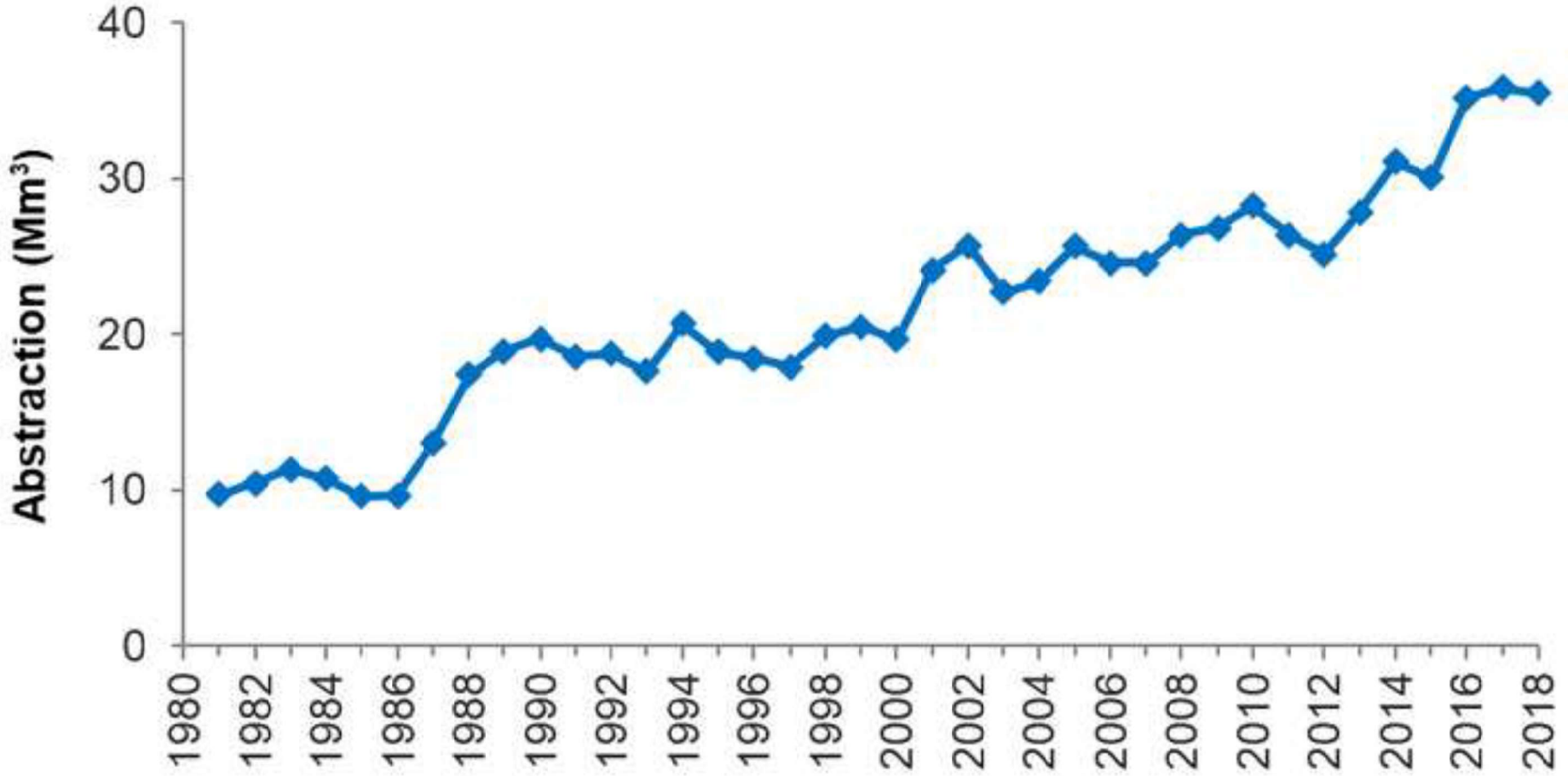

Figure 6

Click here to access/download;Figure;Figure_6.tiff

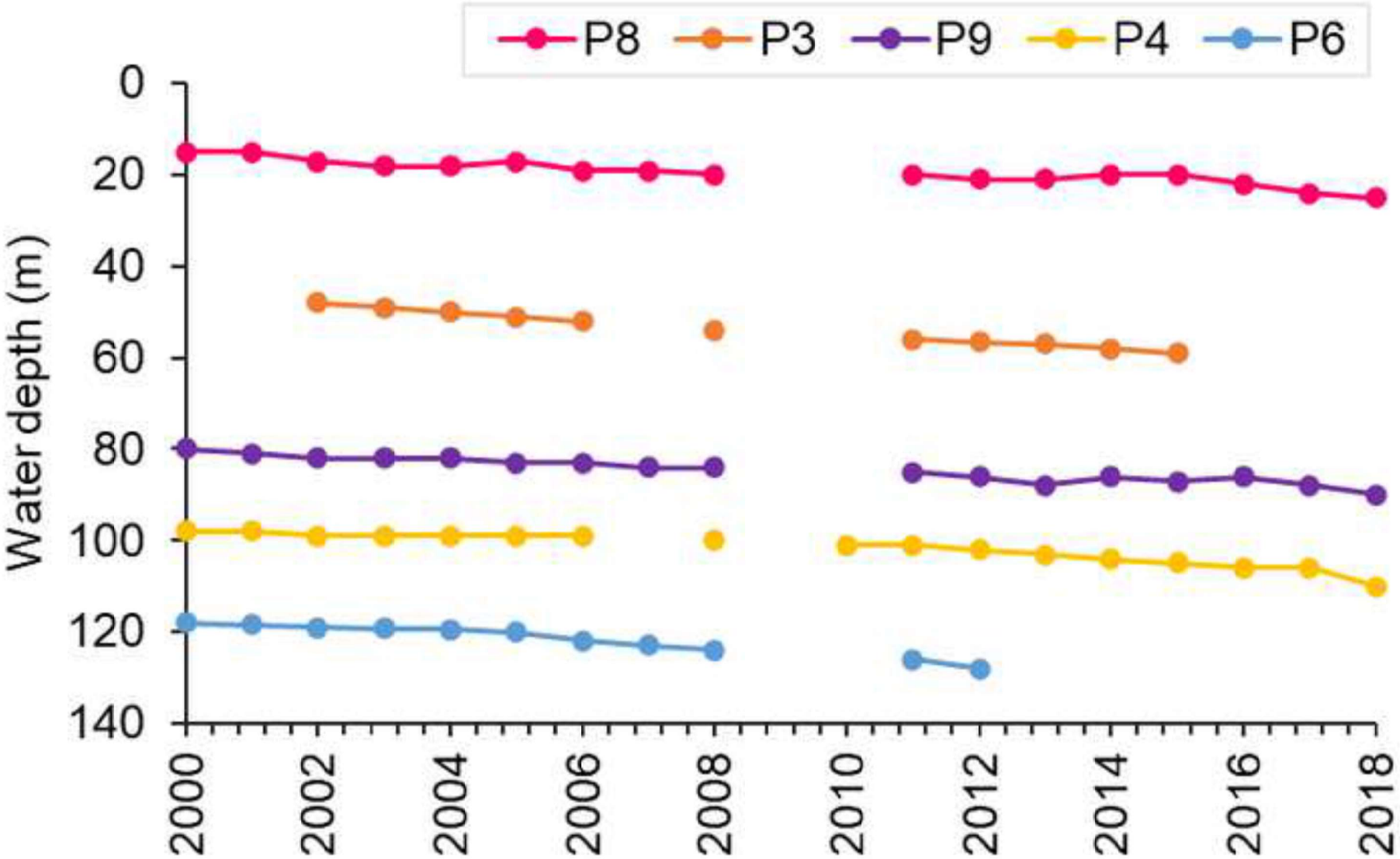

Figure 7

Click here to access/download;Figure;Figure_7.tif

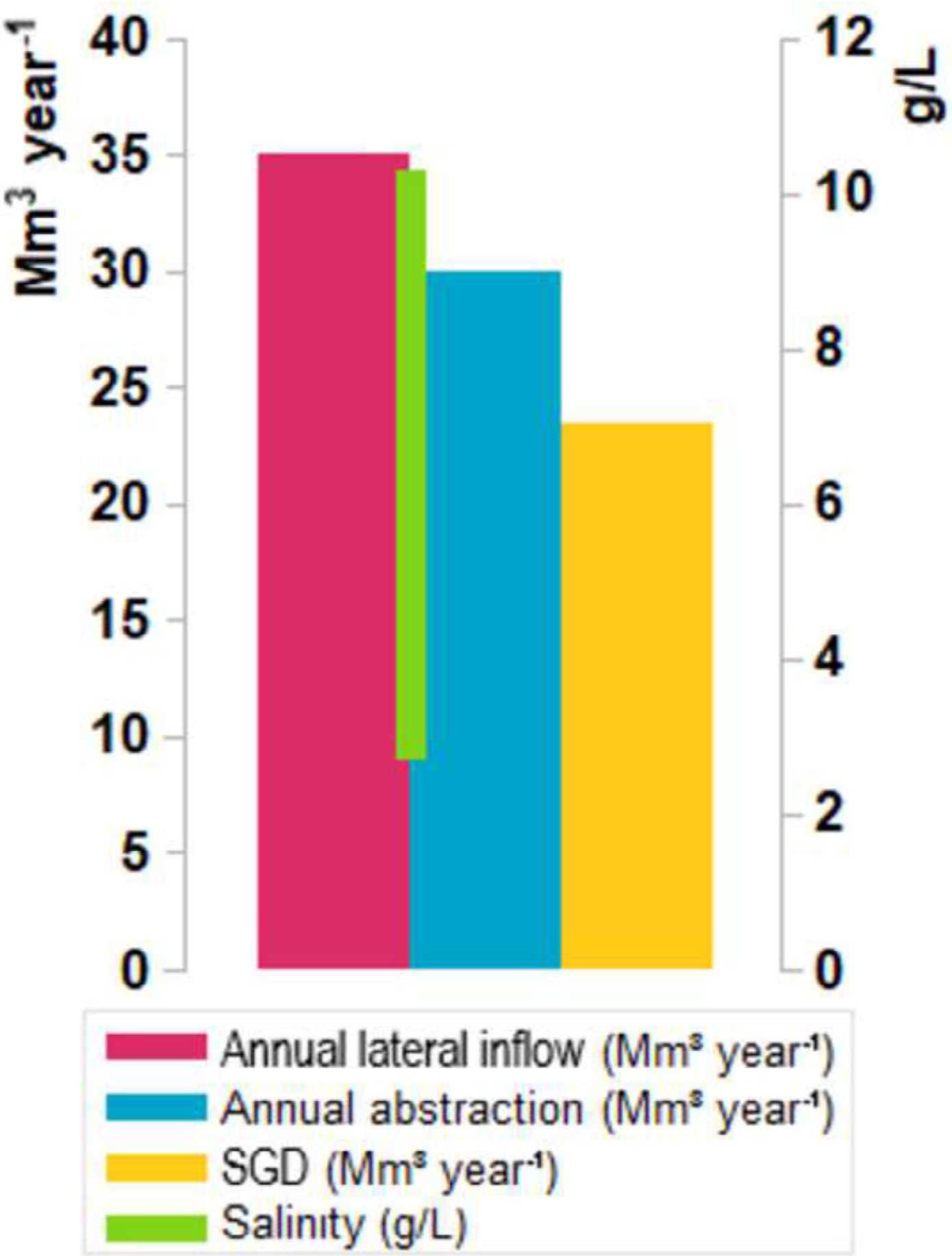

Figure 8

Click here to access/download;Figure;Figure_8.tiff

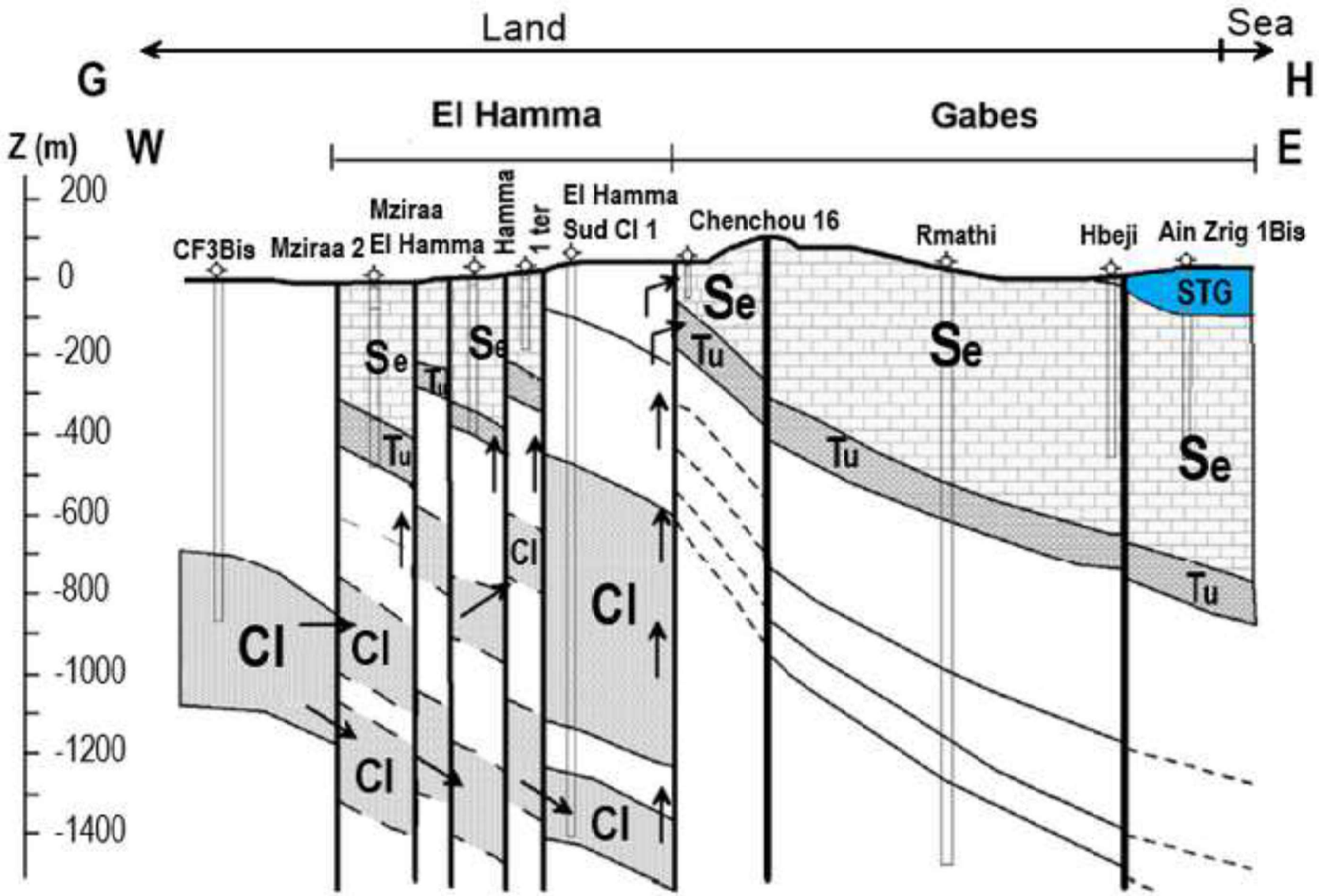

Figure 9

Click here to access/download;Figure;Figure_9.tiff

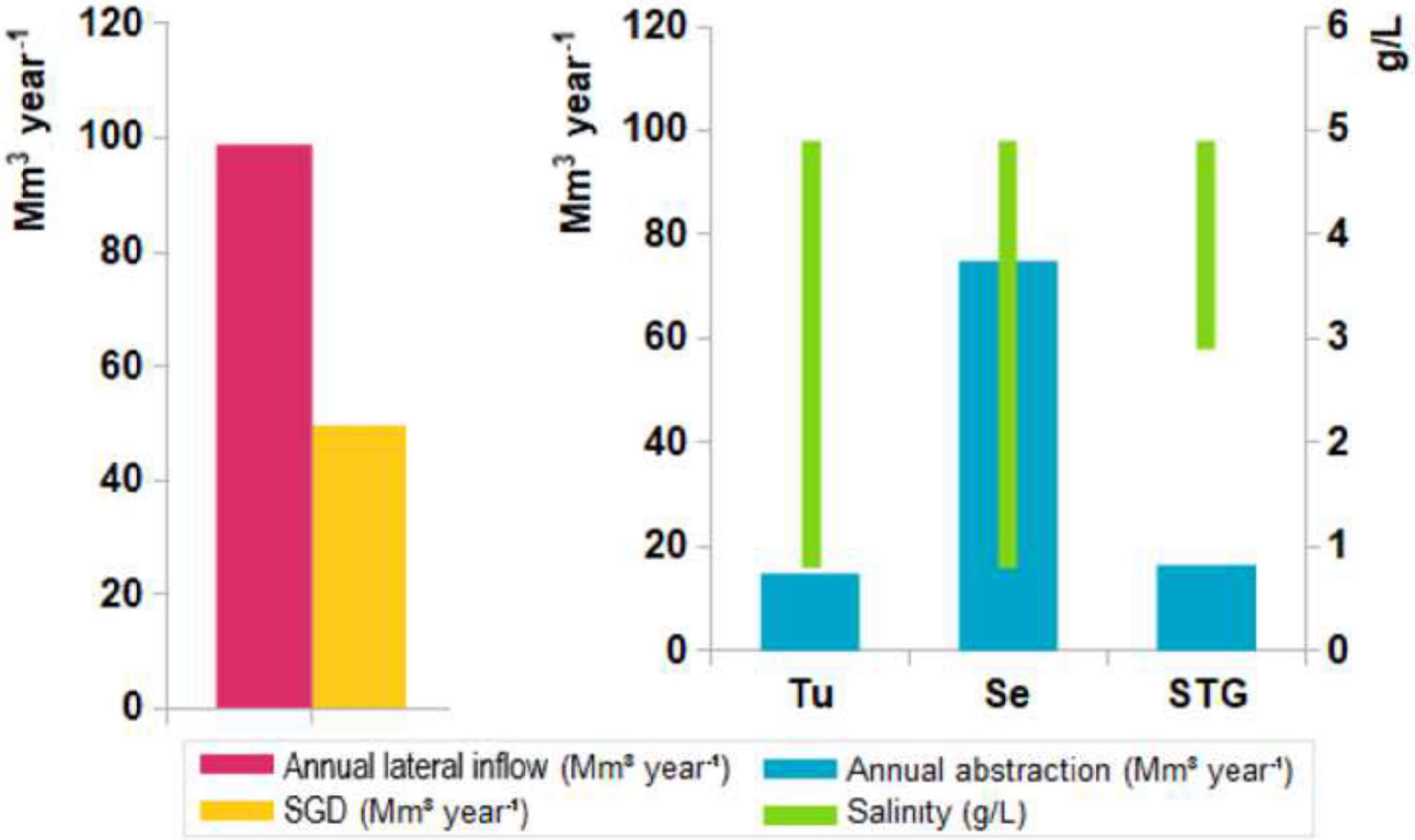

Figure 10

Click here to access/download;Figure;Figure_10.tiff

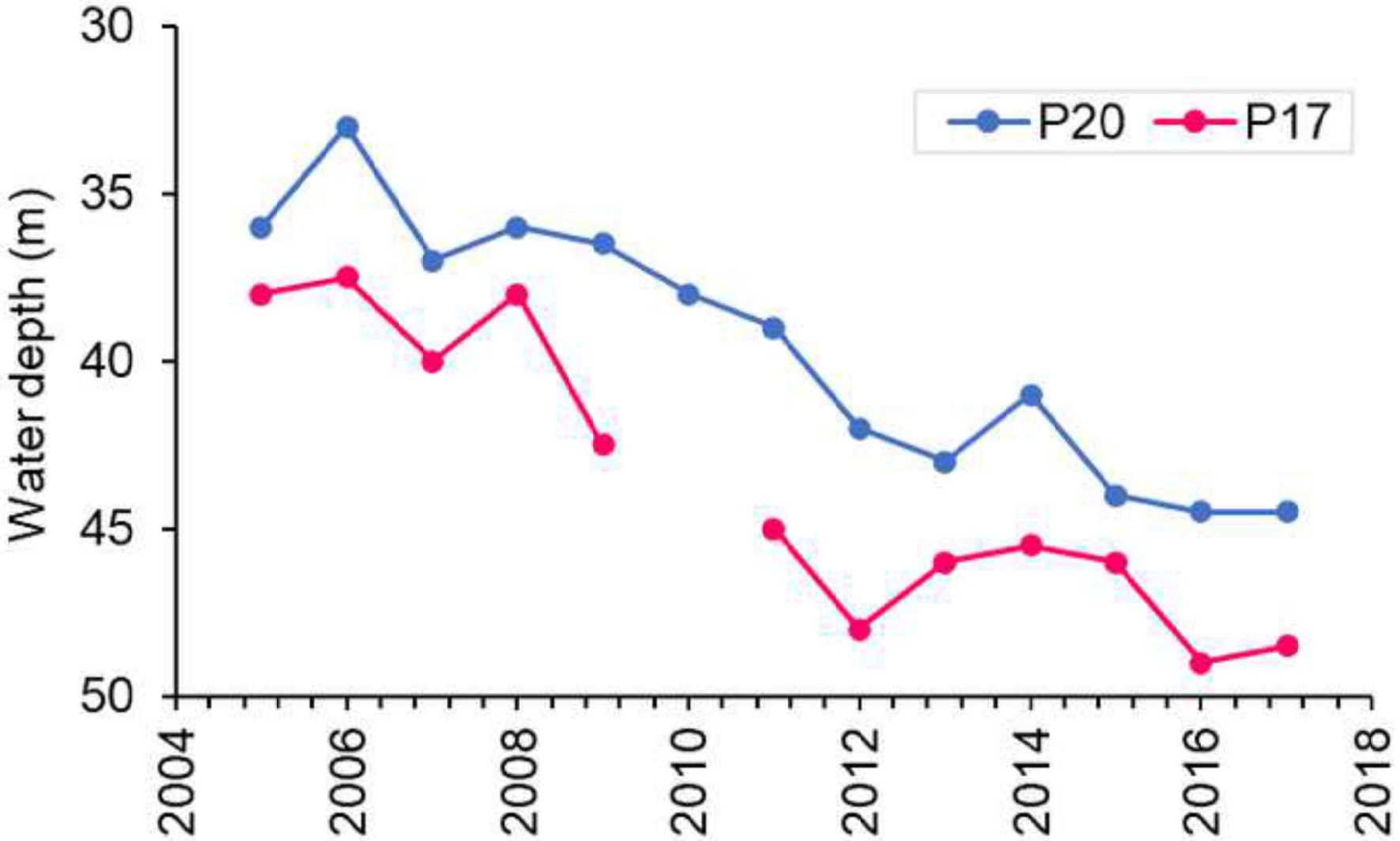

Figure 11

Click here to access/download;Figure;Figure_11.tiff

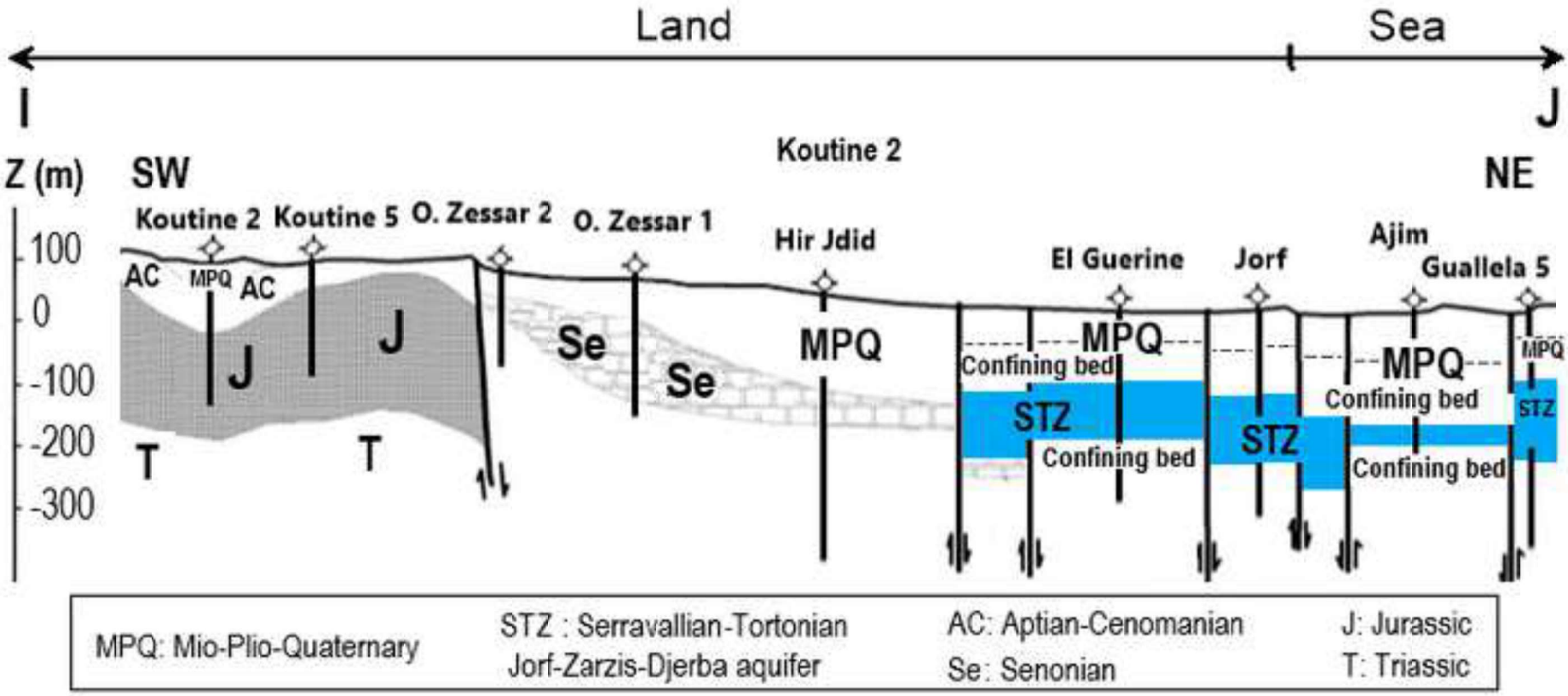

Figure 12

Click here to access/download;Figure;Figure_12.tiff

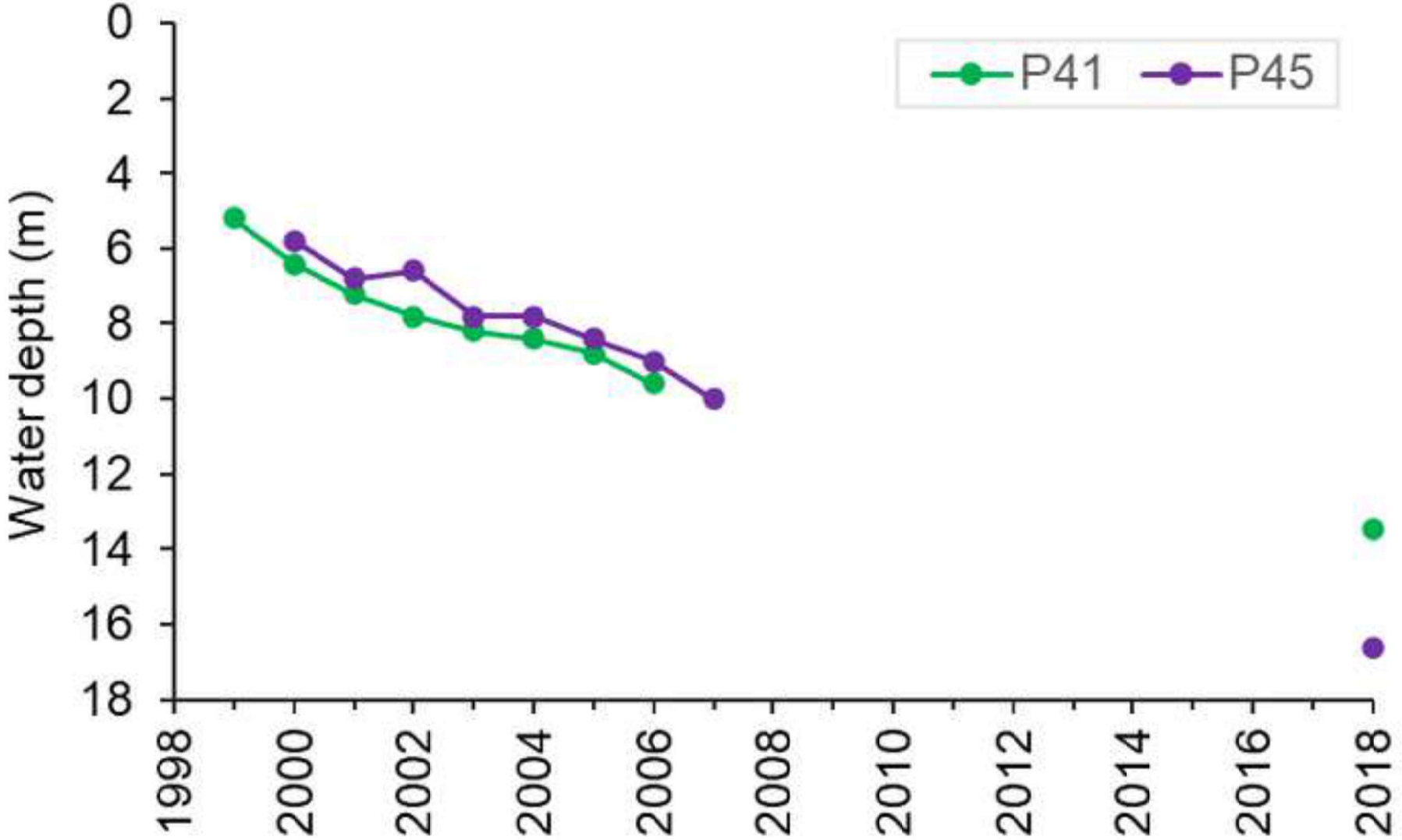

Figure 13

Click here to access/download;Figure;Figure_13.tiff

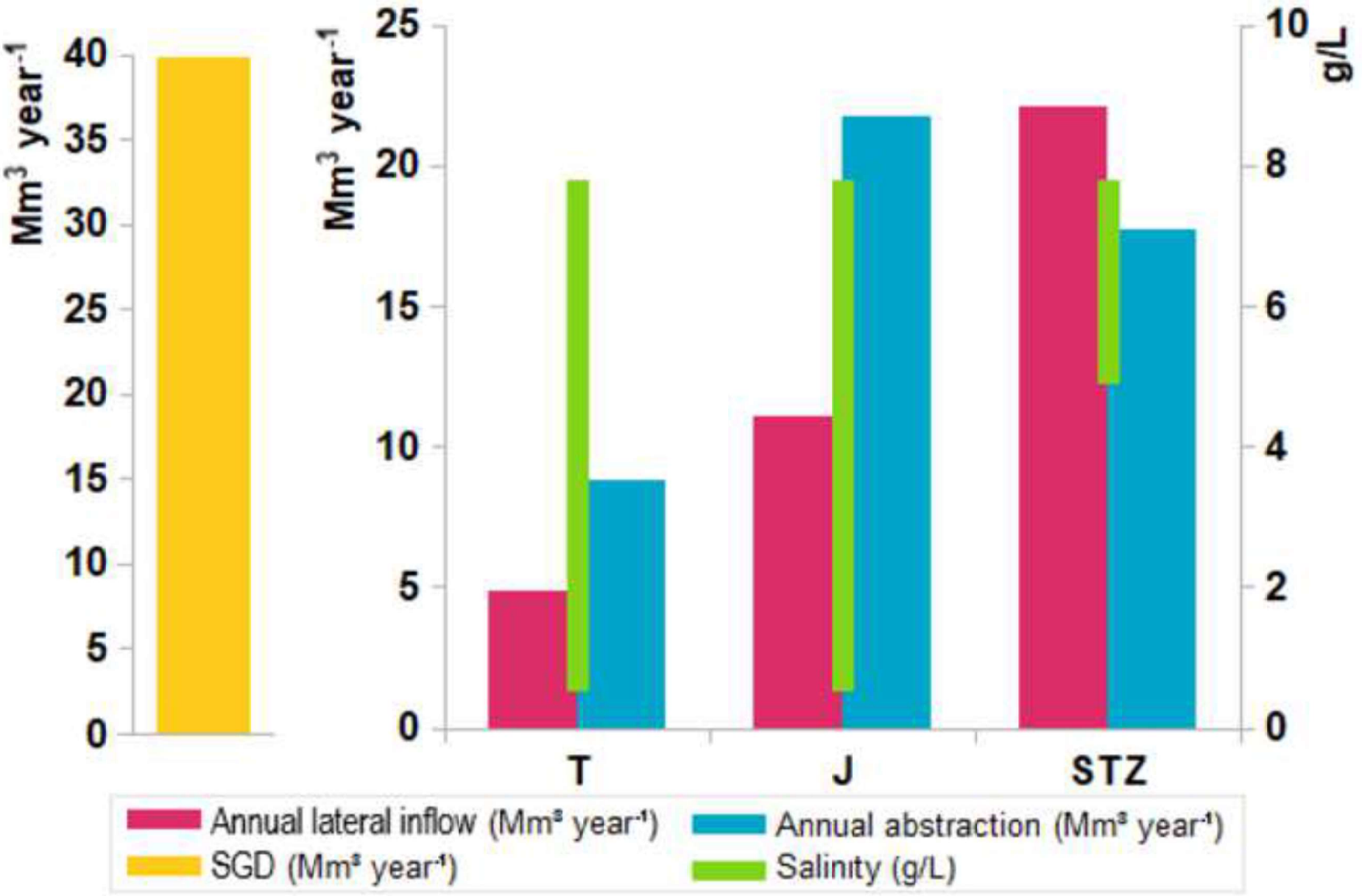

Figure 14

Click here to access/download;Figure;Figure_14.tiff

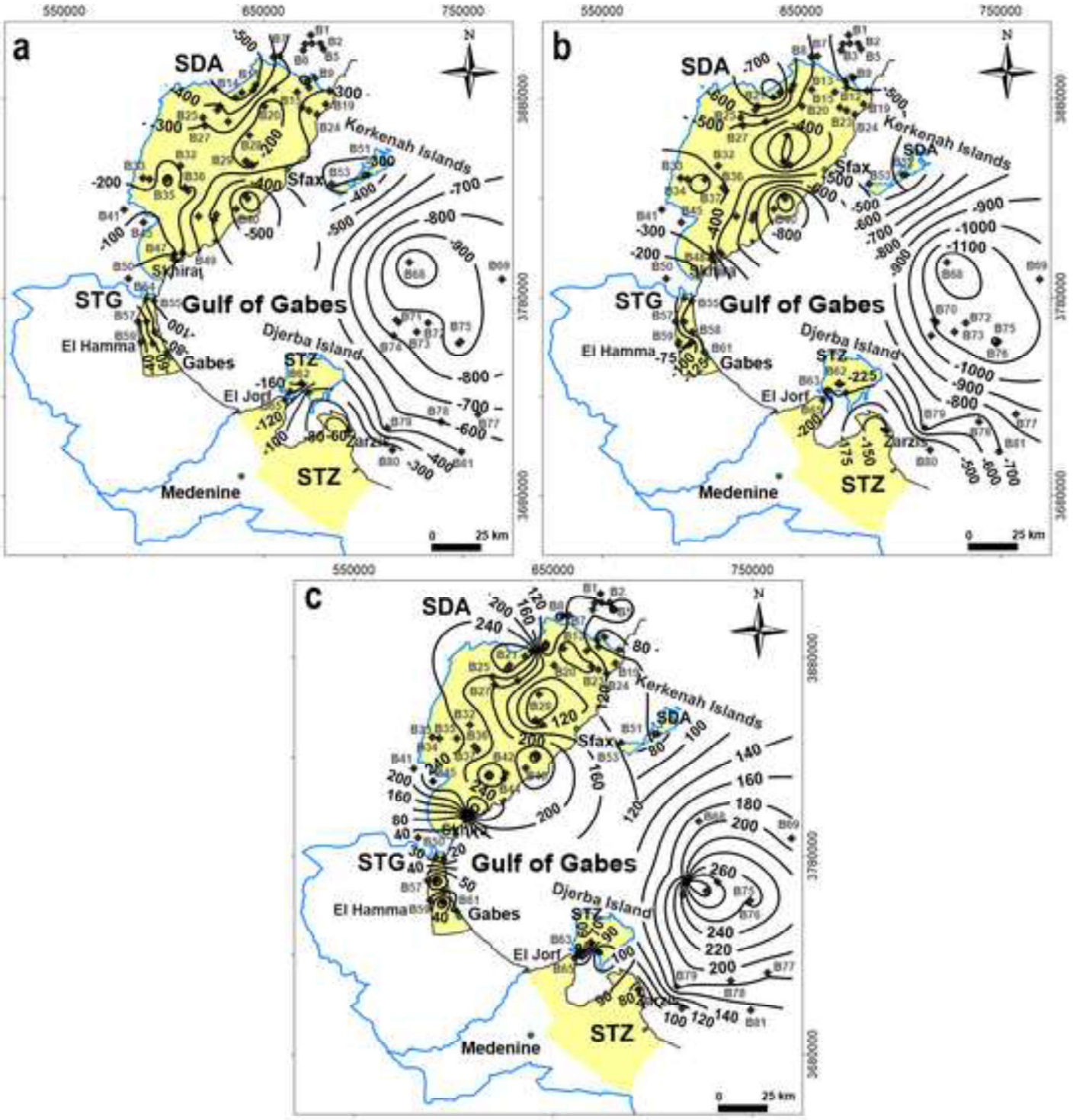

Figure 15

Click here to access/download;Figure;Figure_15.tiff

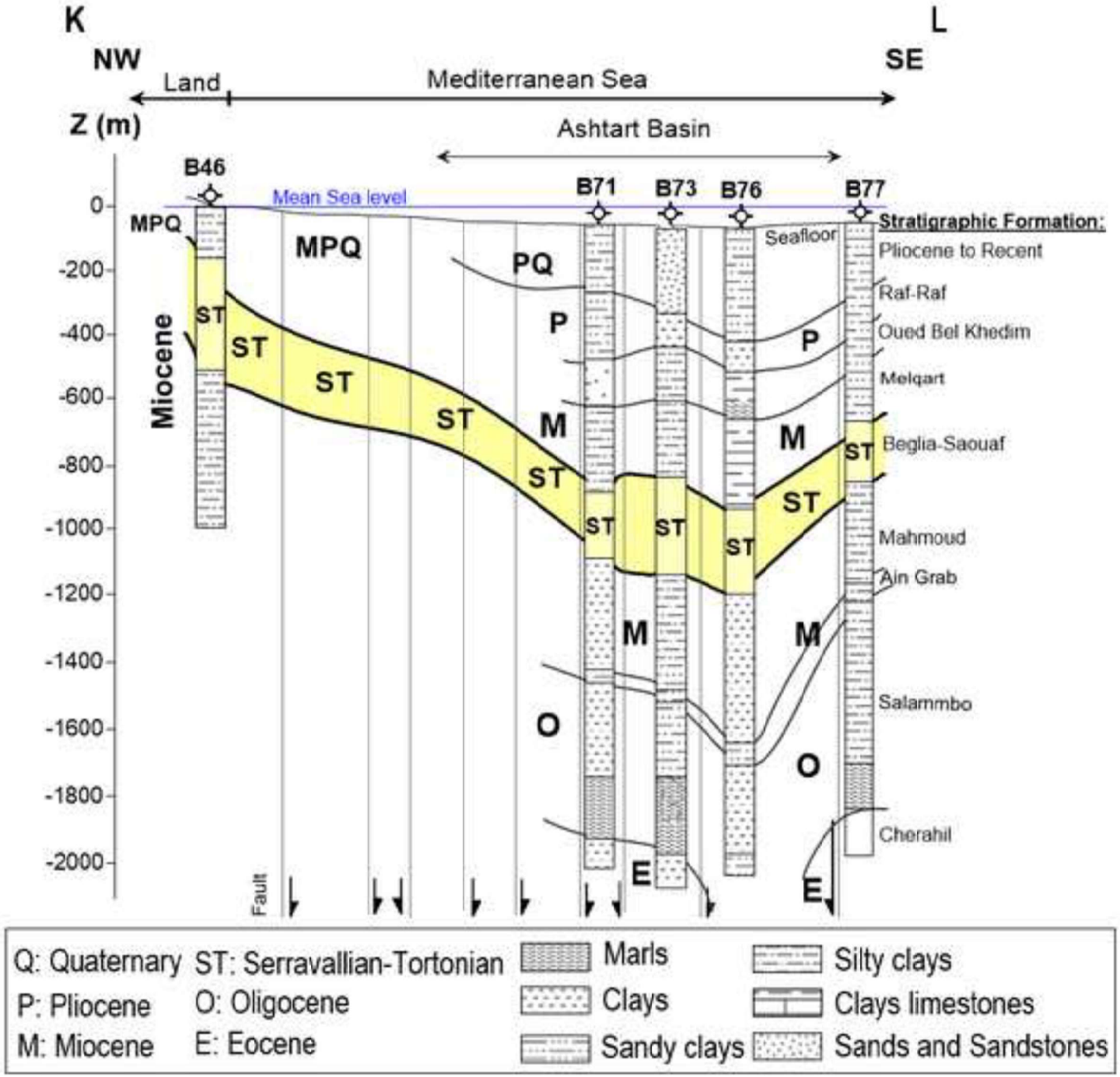

Figure 16

Click here to access/download;Figure;Figure_16.tiff

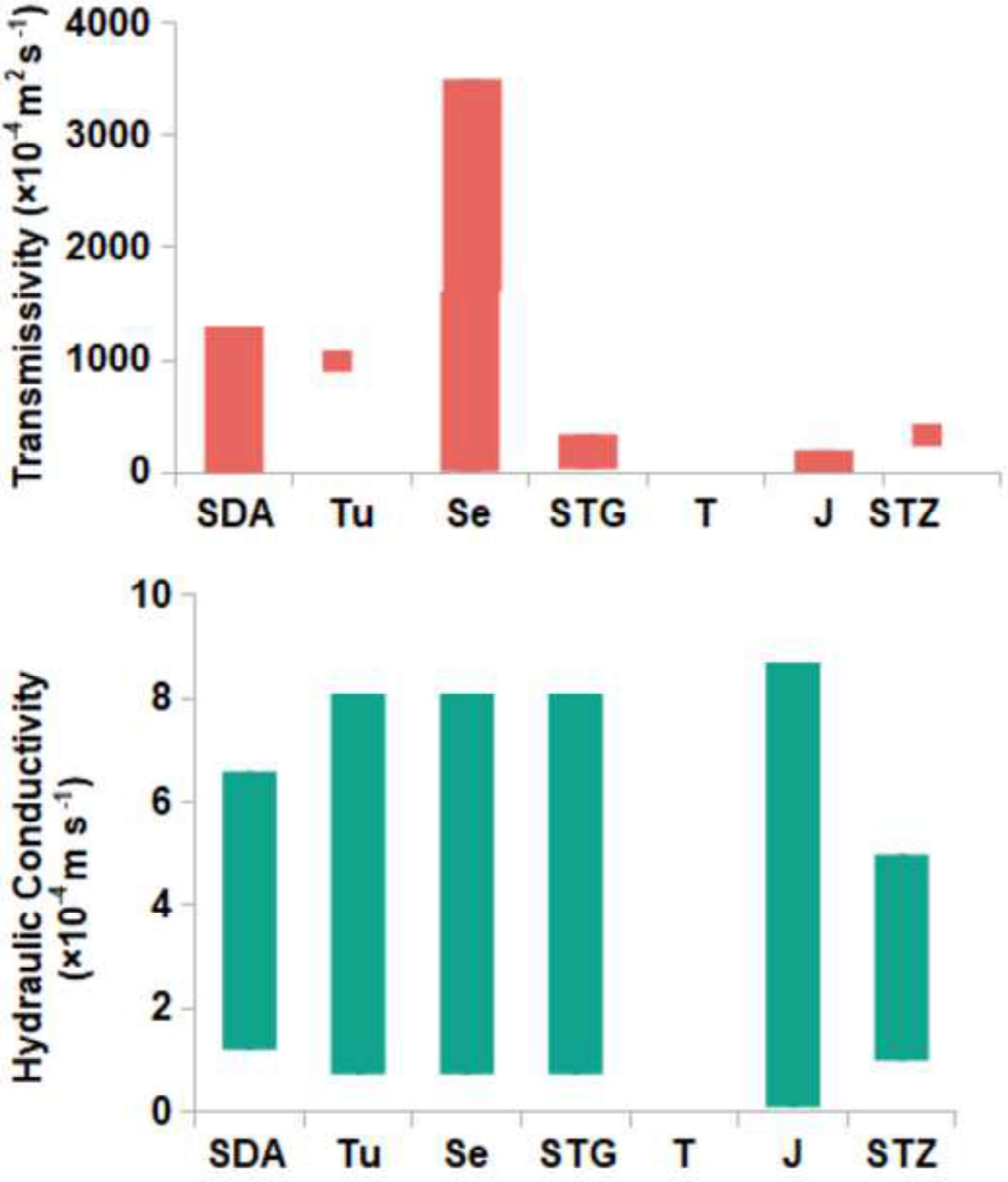

Figure 17

Click here to access/download;Figure;Figure_17.tiff

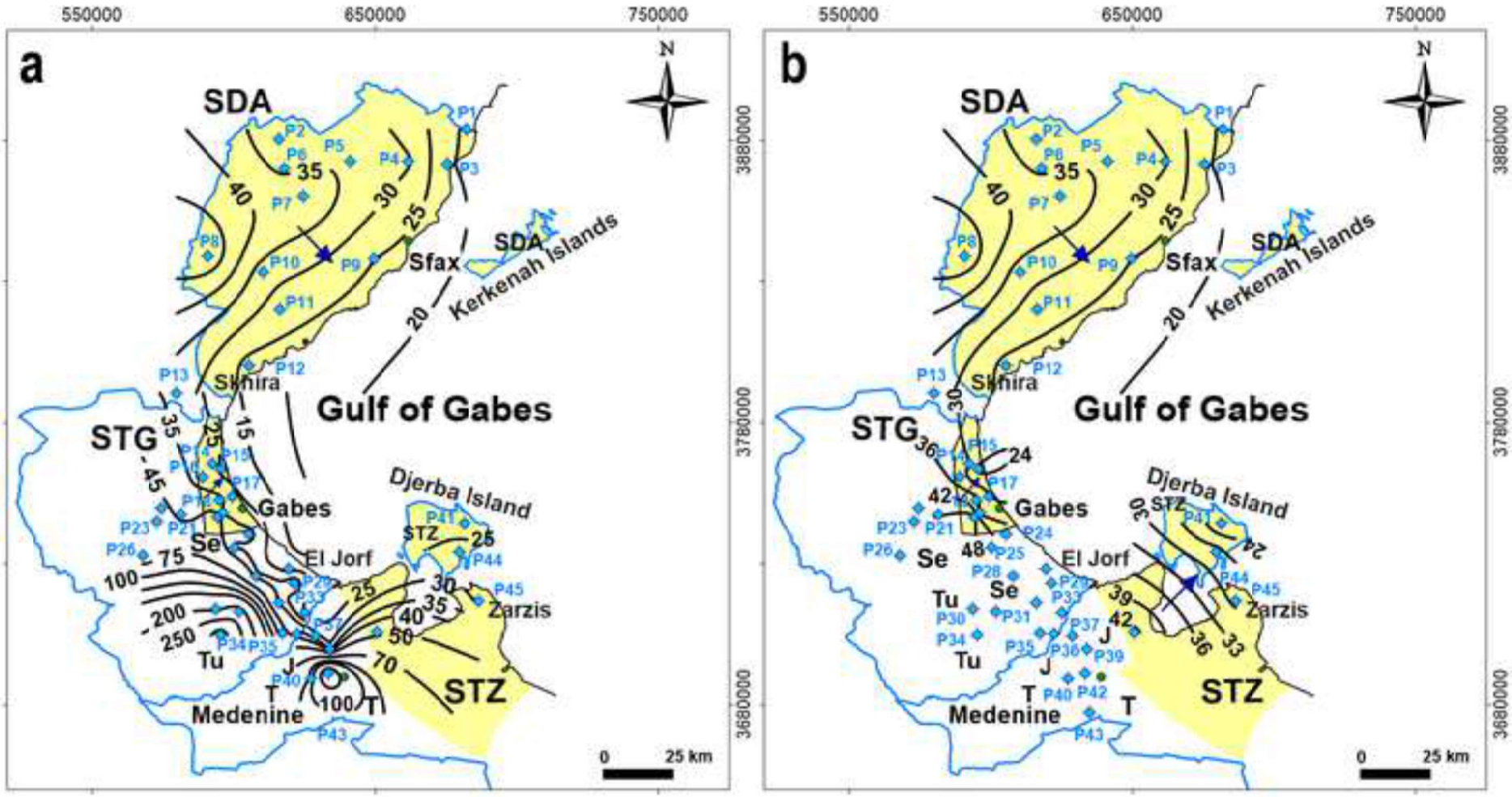

Figure 18

Click here to access/download;Figure;Figure_18.tiff

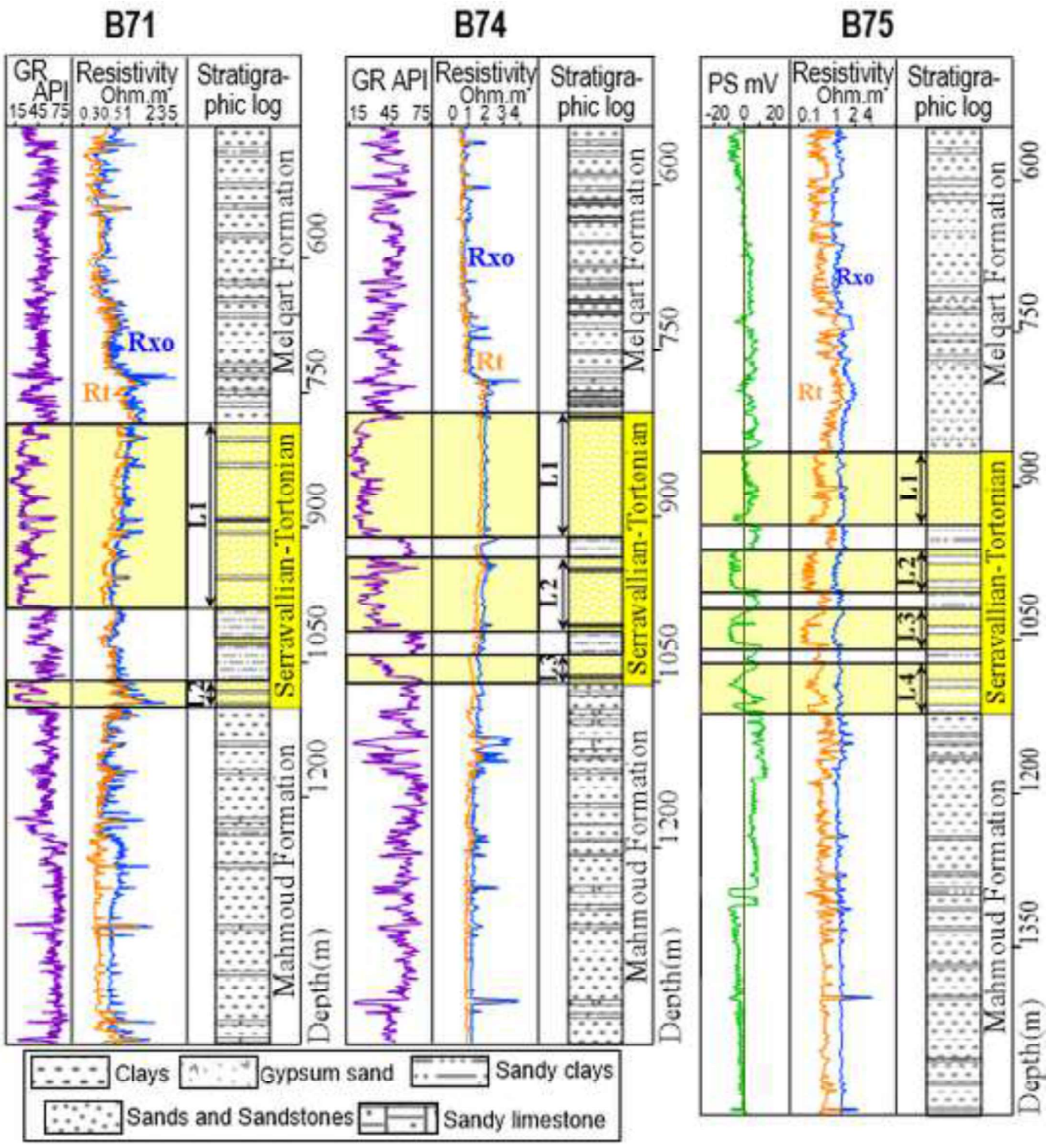

Figure 19

Click here to access/download;Figure;Figure_19.tiff